Journal of Medicinal Chemistry

ARTICLE

pubs.acs.org/jmc

Unprecedented Citrinin Trimer Tricitinol B Functions as a Novel Topoisomerase IIα Inhibitor

Lin Du,[†,∥] Hong-Chun Liu,[‡,∥] Wei Fu,[§,∥] De-Hai Li,[†] Qiu-Ming Pan,[‡] Tian-Jiao Zhu,[†] Mei-Yu Geng,[*,‡] and Qian-Qun Gu[*,†]

[†]Key laboratory of Marine Drugs, the Ministry of Education of China, School of Medicine and Pharmacy, Ocean University of China, Qingdao, 266003, P.R. China

[‡]Division of Antitumor Pharmacology, State Key Laboratory of Drug Research, Shanghai Institute of Materia Medica, Chinese Academy of Sciences, Shanghai 201203, P.R. China

[§]Department of Medicinal Chemistry, School of Pharmacy, Fudan University, Shanghai 201203, P.R. China

Supporting Information

ABSTRACT: Fifteen citrinin derivatives (**1**−**4**, **6**−**16**), including two unprecedented citrinin trimers tricitrinols A (**3**) and B (**4**), were isolated from *Penicillium citrinum* HGY1−5. The six-membered ring A system is essential for the cytotoxicity of active dimers (**1**, **2**, and **5**) and trimers (**3** and **4**). Tricitrinol B (**4**) showed extensive cytotoxicity in 17 tumor cells with comparable low-micromolar IC_{50} values (1−10 μM) and potential antimultidrug resistance capabilities. Tricitrinol B (**4**) induced cell apoptosis in HL60 and HCT116 cells via mainly extrinsic pathways and G2/M arrest. Further antitumor mechanism study and computational docking analysis indicated that tricitrinol B (**4**) works as an intercalating topoisomerase IIα (topo IIα) poison, which inhibits the enzyme activity of topo IIα by interfering predominantly with the topo IIα-mediated poststrand-passage cleavage/religation equilibrium over with the prestrand-passage one and induced DNA damage. Tricitrinol B (**4**) represents a novel class of topo IIα-inhibitory skeletons for developing new chemotherapeutic agents.

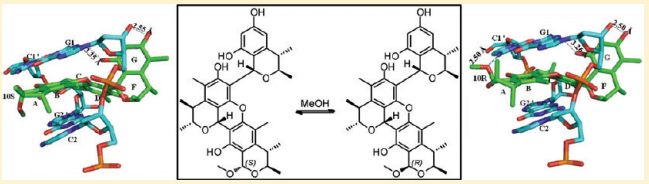

1. INTRODUCTION

DNA topoisomerase II (topo II) is a well-known anticancer target, and topo II inhibitors are among the most effective anticancer drugs currently used in clinical practice.[1,2] Current topo II inhibitors are classified as either topo II poisons or topo II catalytic inhibitors. Topo II poisons act by stabilizing topo II/DNA covalent complex, ultimately generating irreversible DNA double-strand breaks,[3−5] while topo II catalytic inhibitors act at any other stage in the catalytic cycle without generating DNA damage.[6] Most of the current inhibitors, such as etoposide, doxorubicin, and mitoxantrone, are poisons; however, many topo II inhibitors such as adriamycin and its analogues frequently elicit life-threatening toxicities and induce tumor multidrug resistance (MDR), which limit their usage.[7] To overcome these defects, investigators have never stopped searching for novel topo II inhibitors.

Microbial natural products have been a remarkable source of antitumor agents.[8] Since the discovery of antinomycin around 1940, many microbial products have been approved as antitumor drugs including actinomycin D, anthracyclines, bleomycin, mitomycin C, anthracenones, enediynes, and epothilones. New techniques like utilization of uncultivated microorganisms and metagenomics have exhibited great promise to discover new and powerful antitumor drugs.[8] Previous work in our laboratory has been focusing on the discovery of antitumor natural products from marine and terrestrial microorganisms, in combination with cell-based screening assays.[9−13] Over 1000 microorganic lipid extracts were evaluated for cytotoxicity and cell cycle arrest effects in human tumor cells. In a human promyelocytic leukemia HL60 cell-based flow cytometry assay, nearly 90% HL60 cells detected underwent apoptosis following treatment with a lipid extract of a volcano ash isolate of *Penicillium citrinum* HGY1−5 at 10 μg mL^{-1}. Isolation and structure elucidation of the active ethyl acetate extract (27 g) and *n*-butyl alcohol extract (100 g) afforded two unprecedented citrinin trimers tricitrinol A (**3**) and B (**4**), five novel Diels−Alder coupling citrinin dimers dicitrinol A (**1**) and B (**2**), and penicitrinol F−H (**6**−**8**), and eight known analogues penicitrinol B (**9**), penicitrinol A (**10**), penicitrinone A/dicitrinin A (**11**), penicitrinone B (**12**), citrinin (**13**), dihydrocitrinone (**14**), decarboxydihydrocitrinin (**15**), and phenol A (**16**).[14−18] Acidic transformation of dicitrinol A (**1**) afforded an artifact oxodicitrinol A (**5**). All the isolated citrinin derivatives (**1**−**4** and **6**−**16**) were postulated to be artifacts based on the results from comprehensive decomposition studies of citrinin (**13**).

Polyketide mytotoxin citrinin (**13**) is a well-known fungal metabolite which is widely considered as a hazard contaminant of

Received: April 26, 2011
Published: July 15, 2011

Table 1. ^{1}H and ^{13}C NMR Data of Compounds 1, 2, and 5 (600 and 150 MHz, DMSO-d_6, TMS, δ ppm)

	1				2					
	1a (10*S*-isomer)		**1b** (10*R*-isomer)		**2a** (10*S*-isomer)		**2b** (10*R*-isomer)		**5**	
no.	δ_C	δ_H (J in Hz)	δ_C	δ_H (J in Hz)	δ_C	δ_H (J in Hz)	δ_C	δ_H (J in Hz)	δ_C	δ_H (J in Hz)
2	68.8	3.89 qd (6.4, 7.8)	72.3	4.05 q (6.8)	68.8	3.85 qd (6.4, 7.8)	72.3	4.03 q (6.4)	73.1	3.92 qd (6.4, 2.3)
3	36.0	2.67 qd (6.8)	33.9	2.71 q (6.8)	36.1	2.66 qd (6.8, 7.3)	34.2	2.72 q (6.8)	34.9	2.77 qd (6.4, 2.3)
4	139.5		137.8		139.2		137.8		144.3	
5	116.4		115.3		113.1		112.5		118.6	
6	154.4		154.2		148.6		148.3		151.8	
6-OH		8.64 s		8.53 s						
7	103.5		104.7		104.6		104.6		100.9	
8	145.1		145.8		151.3		152.2		146.9	
8-OH						8.38 s		8.28 s		
9	113.1		111.3		115.9		113.9		111.7	
10	94.3	5.56 s	94.1	5.52 s	94.3	5.53 s	94.0	5.38 s	57.4	4.75 s
11	20.2	1.29 d (6.4)	21.7	1.24 d (6.8)	20.5	1.28 d (6.4)	21.8	1.26 d (6.4)	17.5	1.17 d (6.4)
12	19.1	1.14 d (6.8)	20.6	1.11 d (6.8)	19.4	1.09 d (6.8)	20.6	1.07 d (6.8)	19.9	1.18 d (6.8)
13	11.8	2.07 s	9.8	2.07 s	11.5	2.14 s	9.8	2.15 s	10.2	2.14 s
14	54.7	3.45 s	54.9	3.51 s	54.5	3.37 s	54.6	3.42 s		
2′	78.5	4.07 qd (6.4)	78.3	4.08 qd (6.4)	78.3	4.06 qd (6.4)	78.5	4.06 qd (6.4)	81.3	5.05 q (6.8)
3′	36.9	2.88 qd (6.8)	36.9	2.88 qd (6.4)	36.9	2.85 qd (6.8)	37.0	2.85 qd (6.4)	33.9	3.17 q (6.8)
4′	138.1		138.0		138.2		138.3		132.2	
5′	117.5		117.3		117.5		117.5		129.9	
6′	156.1		156.1		156.1		156.1		182.1	
6′-OH		9.61 s		9.61 s		9.64 s		9.64 s		
7′	99.5	6.50 s	99.5	6.47 s	99.4	6.50 s	99.4	6.52 s	101.3	5.98 s
8′	145.9		145.8		146.1		146.1		157.3	
9′	109.1		108.9		109.0		109.0		98.5	
10′	65.7	5.73 s	65.2	5.69 s	65.2	5.64 s	65.3	5.70 s	166.0	
11′	21.6	1.35 d (6.4)	21.7	1.32 d (6.4)	21.7	1.31 d (5.9)	21.6	1.30 d (5.9)	18.1	1.29 d (6.8)
12′	19.7	1.23 d (6.8)	19.7	1.23 d (6.8)	19.8	1.20 d (6.8)	19.9	1.21 d (6.8)	18.6	1.19 d (6.8)
13′	11.0	2.06 s	11.0	2.06 s	11.1	2.05 s	11.0	2.06 s	10.3	1.96 s

food and feeds with multiple toxic effects.[19−21] Mechanism studies revealed that citrinin (**13**) could interfere with electron transport system of mitochondria[22,23] and induce cell apoptosis through the intrinsic pathway.[24] Decomposition of citrinin (**13**) through heating could mainly induce its detoxification via production of some monomeric analogues such as phenol A (**16**) and citrinin H2.[25,26] However, at least one study noted that decomposition of citrinin under aqueous conditions led to an increase in cytotoxicity which is attributed to formation of citrinin H1.[27] Recently, a new class of Diels−Alder coupling citrinin dimers has been discovered from several *Penicillium citrinum* strains.[14−16] Bearing similar coupling penta-ring skeletons, these Diels−Alder dimers did not show obvious in vitro cytotoxicity in several tumor cell lines.[15] In present study, structure−activity relationship of 16 citrinin derivatives for their in vitro cytotoxicity and antitumor mechanism of the novel citrinin trimer tricitrinol B (**4**) will be discussed.

RESULTS AND DISCUSSION

Structure Elucidation of Citrinin Derivatives. Dicitrinol A (**1**) was isolated as a yellowish solid, which displayed strong IR bands at 3419 and 3333 cm^{-1}, indicating the presence of hydroxyl functional groups. A molecular formula of $C_{25}H_{30}O_6$ was assigned based on interpretation of HRESIMS data ($[M - H]^-$ at m/z 425.1954), requiring 11 degrees of unsaturation. The attempts to separate **1** using RP-18 HPLC revealed that it was a mixture of two inseparable and interconvertible analogues (Supporting Information Figure F17). In the ^{1}H and ^{13}C NMR spectra (Table 1, Supporting Information Figure F1 and F2), two sets of resonances were observed, ascribing to two stereoisomers which were present in a ratio of about 2:1. The structure of the major isomer (**1a**) was established by analyses of its 1D (^{1}H and ^{13}C) and 2D (HMQC, $^{1}H-^{1}H$ COSY, and HMBC) NMR spectra (Table 1, Figure 2A). The ^{1}H NMR data of **1a** (Table 1) showed characteristic signals of six methyl groups (δ_H 1.14 (3H, d, J = 6.8 Hz, CH_3-12), 1.23 (3H, d, J = 6.8 Hz, CH_3-12′), 1.29 (3H, d, J = 6.4 Hz, CH_3-11), 1.35 (3H, d, J = 6.4 Hz, CH_3-11′), 2.06 (3H, s, CH_3-13′), and 2.07 (3H, s, CH_3-13)) and a methoxyl group (δ_H 3.45 (3H, s, CH_3-14)). The ^{13}C NMR and DEPT data for **1a** displayed 25 carbon signals comprising seven methyls, seven methines, and 11 quaternary carbons (Table 1). Evaluation of $^{1}H-^{1}H$ COSY correlations between CH_3-11 and H-2, H-2 and H-3, H-3 and CH_3-12, and HMBC correlations originating from H-2 to C-10, from H-3 to C-4, C-5, and C-9, from OH-6 to C-5, C-6, and C-7, from H-10 to C-2, C-4,

dx.doi.org/10.1021/jm200511x |J. Med. Chem. 2011, 54, 5796–5810

Table 2. ^{1}H and ^{13}C NMR Data of Compounds 3 and 4 (600 and 150 MHz, DMSO-d_6, TMS, δ ppm)

			4			
	3		4a (10S-isomer)		4b (10R-isomer)	
no.	δ_C	δ_H (J in Hz)	δ_C	δ_H (J in Hz)	δ_C	δ_H (J in Hz)
2	68.8	3.90 qd (6.4, 7.8)	68.7	3.88 qd (6.4, 7.3)	72.2	4.05 q (6.8)
3	35.9	2.70 qd (6.8, 7.3)	36.0	2.71 qd (6.8, 7.3)	34.1	2.75 q (6.8)
4	139.3		139.1		137.8	
5	116.4		113.3		112.7	
6	154.3		148.6		148.3	
6-OH		8.72 s				
7	103.4		104.7		104.6	
8	145.1		151.2		152.1	
8-OH				8.37 s		8.44 s
9	113.4		115.9		113.9	
10	94.2	5.75 s	94.3	5.55 s	94.0	5.42 s
11	20.3	1.29 d (6.4)	20.5	1.29 d (6.4)	21.7	1.24 d (6.4)
12	19.3	1.15 d (6.4)	19.4	1.14 d (6.8)	20.7	1.11 d (6.8)
13	11.9	2.09 s	11.5	2.22 s	9.8	2.23 s
14	54.4	3.35 s	54.5	3.39 s	54.6	3.43 s
2′	78.4	4.08 qd (6.4)	78.1	4.08 qd (6.4)	78.3	4.08 qd (6.4)
3′	36.8	2.87 qd (6.8)	36.8	2.85 qd (6.8, 6.4)	36.9	2.85 qd (6.4, 6.4)
4′	136.5		136.4		136.5	
5′	117.4		117.2		117.2	
6′	154.1		153.9		153.9	
6′-OH		6.73, s		6.65 s		6.65 s
7′	112.7		112.7		112.7	
8′	144.8		144.7		144.7	
9′	109.8		109.5		109.5	
10′	66.4	5.79, s	65.6	5.75 s	65.7	5.77 s
11′	21.5	1.37 d (6.4)	21.6	1.35 d (6.4)	21.6	1.32 d (6.4)
12′	19.8	1.21 d (6.8)	19.9	1.23 d (6.8)	20.0	1.23 d (6.8)
13′	11.3	1.97 s	11.3	1.97 s	11.2	1.97 s
2″	72.7	3.84 qd (6.8, 2.8)	72.8	3.94 q (6.8)	72.2	3.94 q (6.8)
3″	35.2	2.66 qd (6.8, 2.8)	34.8	2.66 q (6.8)	34.9	2.66 q (6.8)
4″	138.2		138.1		138.1	
5″	112.9		113.4		113.3	
6″	155.4		155.2		155.3	
6″-OH		9.15 s		9.14 s		9.14 s
7″	100.4	6.22 s	100.6	6.21 s	100.6	6.21 s
8″	151.8		151.8		151.8	
8″-OH		9.02 s		8.95 s		8.97 s
9″	111.3		111.2		111.2	
10″	62.8	6.38 s	62.1	6.41 s	62.1	6.43 s
11″	19.2	1.22 d (6.4)	19.6	1.22 d (6.4)	19.6	1.22 d (6.4)
12″	18.8	1.29 d (6.4)	17.3	1.29 d (6.4)	17.4	1.29 d (6.4)
13″	10.4	2.01 s	10.1	2.02 s	10.1	2.02 s

C-8, C-9, and CH_3-14, from CH_3-13 to C-4, C-5, and C-6, and from CH_3-14 to C-10 revealed the substructure of moiety A (Figure 2A). Analysis of the rest of the 2D NMR signals could establish a substructure of moiety B (Figure 2A). The connection of C-7 and C-10′ was confirmed by the HMBC correlations originating from H-10′ to C-6, C-7, and C-8 (Figure 2A). The bridging of C-8 and C-8′ through an oxygen atom was deduced by analysis of the ^{13}C NMR data for C-8 (δ 145.1) and C-8′ (δ 145.9) and the degree of unsaturation. The planar structure of the minor isomer (**1b**), elucidated by the analyses of its 1D and 2D NMR resonances (Table 1, Figure 2A), was the same as that of **1a**.

Dicitrinol B (**2**) was isolated as a yellowish solid. The same molecular formula of $C_{25}H_{30}O_6$ as that of **1** was established by HRESIMS. It was also a mixture of two inseparable isomers which were present in a ratio of 5:7 (Table 1, Supporting

dx.doi.org/10.1021/jm200511x |J. Med. Chem. 2011, 54, 5796–5810

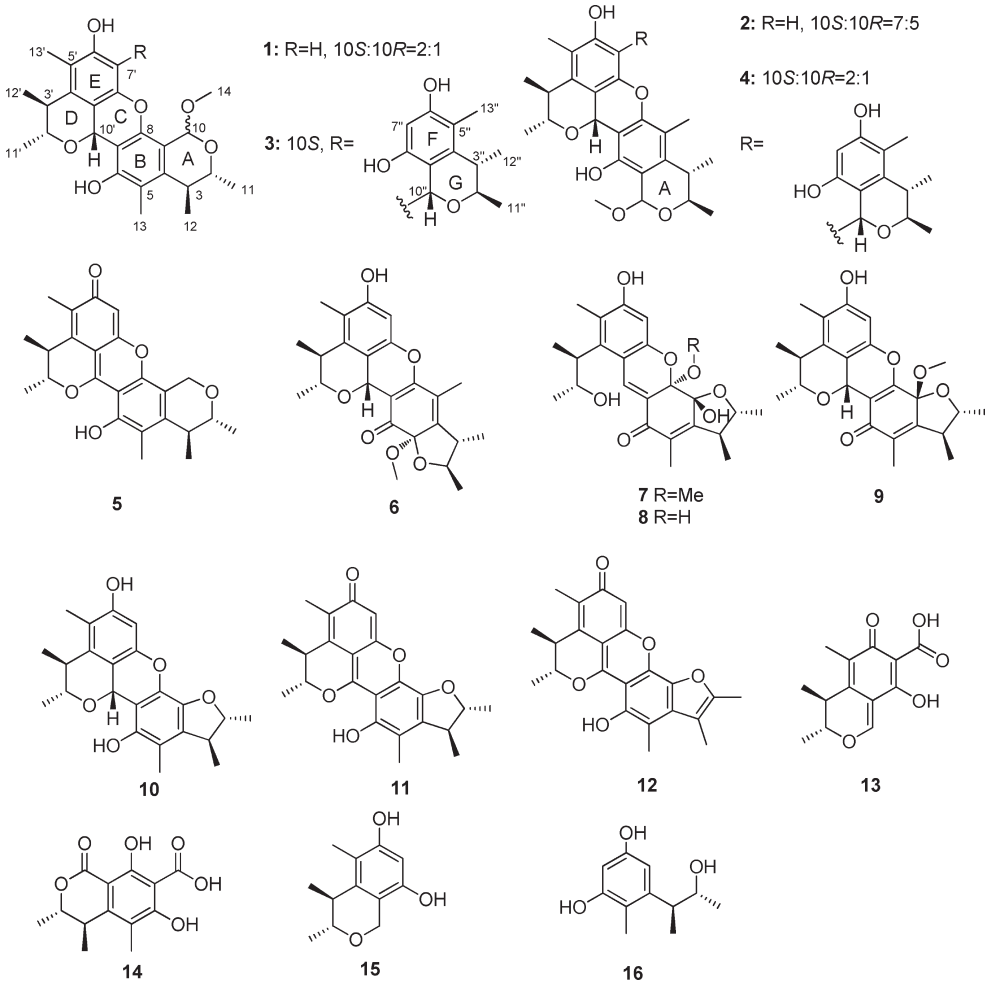

Figure 1. Structures of compounds **1**−**16**.

Information Figure F18). The ^{1}H and ^{13}C NMR data of the major isomer (**2a**) was almost identical to those of **1a** (Table 1) except that C-5/C-6 upfield shifted and C-8/C-9 downfield shifted in **2a**. It indicated that they had the same structure, except that the oxygen bridge connecting C-6 with C-8′ in **2a** (Figure 1). It was further confirmed by analyses of HMBC correlations from H-10 to C-8 (δ 151.3), C-9 (δ 115.9), and C-4(δ 139.2), from CH_3-13 to C-6 (δ 148.6), C-5 (δ 113.1), and C-4, and from H-10′ to C-6, C-7, and C-8 (Figure 2A). Similarly the planar structure of the minor isomer (**2b**) was elucidated the same as that of **2a.**

Tricitrinol A (**3**) was obtained as a yellowish solid. Its molecular formula was established as $C_{37}H_{44}O_9$ by HRESIMS, requiring 16 degrees of unsaturation. Comparison of ^{1}H and ^{13}C NMR data (Table 2) with those of **1a** and **1b** (Table 1) indicated that there was a 7′-substituted-**1a** substructure in **3** (Figure 2A). The rest spectral data indicated the presence of a moiety C, which was similar to moiety B and confirmed by analyses of the 2D NMR (HMQC, $^{1}H-^{1}H$ COSY and HMBC) spectra (Figure 2A). On the basis of HMBC correlations from H-10″ to C-6′, C-7′, and C-8′, moiety C was linked to moiety B through a single bond between C-7′ and C-10″. So the structure of **3** was established as a novel citrinin trimer.

Tricitrinol B (**4**) was obtained as a yellowish solid. Its molecular formula was determined as $C_{37}H_{44}O_9$ by HRESIMS, which was identical to that of **3**. It was identified as a mixture of two isomeric citrinin trimers (ratio of 2:1, Supporting Information Figure F20) by comparison of its physicochemical properties and spectroscopic data (^{1}H and ^{13}C NMR) (Table 1 and 2) with those of **1**−**3**. Further comparison of the 1D NMR data of the two isomers (**3a** and **3b**) with those of **1**−**3** (Table 1 and 2) could establish their planar structures as shown in Figure 1.

The absolute configurations of compounds **1**−**4** were established by a combination of chemical and spectroscopic methods. HPLC-PDA-MS analyses of fresh *n*-BuOH extract detected none of the four compounds (Supporting Information Figure F22A). After a long-term storage, compounds **1**−**4** appeared accompanying a decrease of citrinin (**13**) (Supporting Information Figure F22B). It is reasonable to assume that compounds **1**−**4** could be produced through artificial polymerization of citrinin (**13**). It was further confirmed by chemical transformation of citrinin (**13**) into **1** and **2** in MeOH (Supporting Information Figure F23). So the absolute configurations of C-2/2′/2″ and C-3/3′/3″ in **1**−**4** could be deduced as *R* and *S*, respectively, consistent with those in **13**.[17] On the basis of NOESY correlations between OCH_3-14 and H-2, between H-10′ and H-2′, CH_3-12′, between OCH_3-14 and H-10″, CH_3-11″, and between CH_3-12″ and OH-6′ (Figure 2B), the absolute configurations of C-10, C-10′, and C-10″ in **3** were deduced as *S*, *R*, and *S*, respectively. The absolute configurations of C-10′ in **1** and **2** and those of C-10′ and C-10″

dx.doi.org/10.1021/jm200511x |*J. Med. Chem.* 2011, 54, 5796–5810

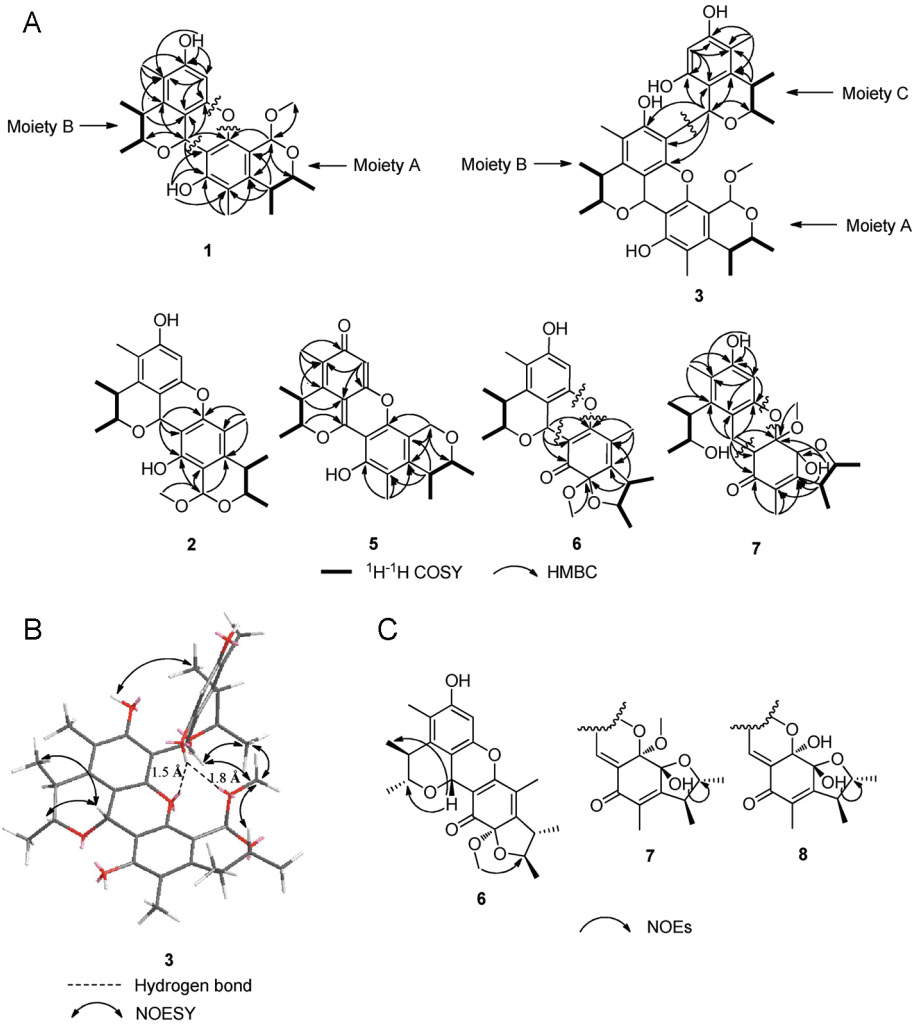

Figure 2. Selected 2D NMR correlations of **1**−**8**. (A) Key ^{1}H−^{1}H COSY and HMBC correlations of compounds **1**−**3** and **5**−**7**. (B) Key NOESY correlations of **3**. (C) Key NOEs correlations of **6**−**8**.

in **4** were determined the same as those in **3** because of their nearly identical ^{1}H and ^{13}C NMR data for rings D-G (Table 1 and 2).

Citrinin (**13**) could undergo C-10 epimerization via a reversible 1−4, Michael type, nucleophilic addition of methanol or water (Figure 3A).[28−30] Further comparison of the 1D NMR data of the moieties A in the two isomers of **1**, **2**, and **4** (Table 1 and 2) with those of the citrinin (**13**) adducts[28−30] indicated that **1**, **2**, and **4** were mixtures of two C-10 epimers formed by a reversible nucleophilic addition of methanol, respectively (Figure 3B). The absolute configurations of C-10 in the major epimers (**1a**, **2a**, and **4a**) and the minor ones (**1b**, **2b**, and **4b**) were determined to be *S* and *R*, respectively.[28−30] A molecular model (Chembio3D Ultra 11.0 software, using the MM2 minimizing method) of **3** afforded a stable confirmation that was consistent with the NOESY correlations (Figure 2B). Strong innermolecular hydrogen bonds of a hydrogen atom of OH-6″ with two oxygen atoms of ring C and OCH_3-14 could lock the *S* configuration of C-10 and block the epimerization of **3** in MeOH.

Compounds **1**−**4** were unstable in acidic conditions, and their solution (in MeOH, DMSO, etc.), when exposed to acid (TFA, etc.), turned into dark-yellow/red quickly. To a suspension of 30 mg of **1** in 0.5 mL DMSO was added 50 μL of TFA at room temperature. A major product, oxodicitrinol A (**5**), was obtained as a yellow solid. Its UV spectrum showed absorption maxima at λ_{max} (log ε) 234 (4.23), 262 (4.22), 316 (3.75), 400 (4.02), and 418 (4.02) nm in MeOH, implying presence of large conjugated system. Its molecular formula $C_{24}H_{26}O_5$ was determined by HRESIMS. Its ^{1}H and ^{13}C NMR data were quite different from those of **1** (Table 1). Signals for OCH_3-14 were absent, but resonances for a methylene CH_2-10 (δ_H 4.75, s, 2H; δ_C 57.4) were observed in ^{1}H and ^{13}C NMR spectra of **5**. Moiety B transformed from a phenol type to a quinine type, which was identical to that in dicitrinin A (**11**).[14] The structure of **5** was further confirmed by analyses of its 2D (HMQC, ^{1}H−^{1}H COSY, and HMBC) NMR correlations (Figure 2A).

Compound **6** had the same molecular formula, $C_{24}H_{28}O_6$, established by HRESIMS (*m*/*z* 413.1955 $[M + H]^+$, calcd 413.1964), as the known citrinin dimer penicitrinol B (**9**).[16] Careful comparison of their 1D NMR data[16] (Table 3) indicated that they had a same substructure of moiety B but differed in the structure of ring B and the conjunction pattern of the two moieties. Analyses of ^{13}C shifts of C-6 (δ 158.9), C-7 (δ 104.7), and C-8 (δ 191.2), together with the key HMBC

dx.doi.org/10.1021/jm200511x |*J. Med. Chem.* 2011, 54, 5796–5810

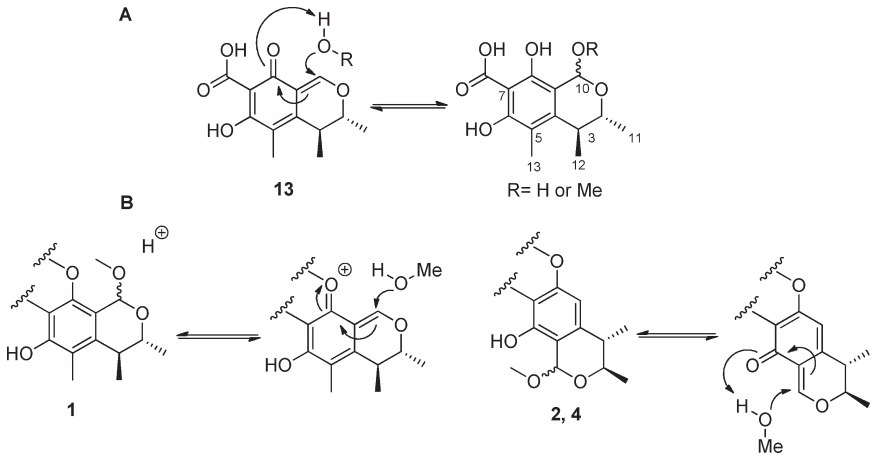

Figure 3. Reversible nucleophilic addition mechanisms of citrinin (**13**) (A), dicitrinol A (**1**), dicitrinol B (**2**), and tricitrinol B (**4**) (B).

Table 3. ^{1}H and ^{13}C NMR Data of Compounds 6−8 (600 and 150 MHz, DMSO-d_6, TMS, δ ppm)

	6		7		8	
no.	δ_C	δ_H (J in Hz)	δ_C	δ_H (J in Hz)	δ_C	δ_H (J in Hz)
2	81.1	3.91 qd (5.9, 6.4)	80.6	4.03 qd (6.4)	80.8	4.06 qd (6.4)
3	41.7	2.57 qd (6.4, 6.9)	42.4	2.59 qd (6.8)	42.6	2.57 qd (6.8)
4	149.0		158.6		158.1	
5	121.1		126.5		126.9	
6	158.9		185.6		185.5	
7	104.7		118.8		122.2	
8	191.2		98.2		94.6	
8-OH						6.18 s
9	98.8		100.6		100.3	
9-OH				6.21 s		6.05 s
10	19.4	1.29 d (5.9)	19.4	1.31 d (6.4)	19.3	1.34 d (6.4)
11	17.0	1.21d (6.9)	16.2	1.21 d (6.4)	16.3	1.22 d (6.8)
12	11.6	1.92 d (0.9)	11.3	1.75 s	11.3	1.76 s
13	49.1	3.08 s	50.7	3.02 s		
2′	78.4	3.81 m (5.9, 5.0)	70.5	4.06 m	70.6	4.02 m
2′−OH				4.36 brs		4.22 brs
3′	37.2	2.81 m (6.9, 5.0)	43.2	3.20 m	43.4	3.20 m
4′	139.9		145.2		145.0	
5′	119.5		117.8		117.5	
6′	155.7		158.8		158.5	
6′−OH		9.80 s		10.08 s		9.94 s
7′	99.1	6.49 s	100.0	6.44 s	101.5	6.39 s
8′	144.4		153.4		151.9	
9′	110.4		108.5		109.4	
10′	61.2	5.13 s	130.6	8.07 s	128.3	7.86 s
11′	22.3	1.16 d (5.9)	23.1	1.22 d (6.4)	22.9	1.23 d (6.8)
12′	20.6	1.20 d (6.9)	18.0	1.23 d (6.4)	18.0	1.24 d (6.8)
13′	10.6	2.05 s	11.5	2.09 s	11.6	2.09 s

correlations from H-10′ to C-6, C-7, and C-8, and from CH_3-12 to C-6, confirmed that ring B turned to a cyclohexa-2,4-dienone and the oxygen bridge should connect C-8′ with C-6. In a different NOE experiment, NOE correlations of OCH_3-13 with H-2 and those of H-10′ with H-2′ and CH_3-12′ established the relative configurations on rings A and D, respectively. (Figure 2C).

Penicitrinol G (**7**) was obtained as a yellow solid. The ion peak at m/z 429.1905 $[M - H]^-$ in the HRESIMS established the molecular formula as $C_{24}H_{30}O_7$. Analyses of a ^{1}H−^{1}H COSY spin system from CH_3-10 to CH_3-11 and HMBC correlations from H-3 to C-4 and C-5, from H-10′ to C-6, C-7, and C-8, from CH_3-12 to C-4, C-5, and C-6, from CH_3-13 to C-8, and from OH-10 (OH-9) to C-4, C-8, and C-9 could establish a moiety A (Figure 2A). Analyses of the rest 2D NMR correlations could give a moiety B (Figure 2A). Comparing with the structure of **9**, ring C opened and a 7,10′-double bond formed which was confirmed by the presence of OH-2′ (δ 4.36, brs) resonance in ^{1}H NMR spectrum of **7** together with HMBC correlations form H-10′ (δ 6.44, s) to C-6, C-7, C-8, C-4′, C-8′, and C-9′ (Figure 2A). C-8 (δ 98.2) and C-8′ (δ 153.4) were connected via an oxygen bridge, confirmed by analysis of their ^{13}C NMR data and the degree of unsaturation. The difference NOE experiment of **7** showed association between OH-9 (δ 6.21) and H-2 (δ 4.03). No correlation was observed between OCH_3-13 (δ 3.02) and OH-9 (Figure.2C). Thus the relative configurations of OH-9/H-2 and OH-9/OCH_3-13 were proposed as *cis* and *trans*, respectively.

The molecular formula of penicitrinol H (**8**), assigned as $C_{23}H_{28}O_7$ by HRESIMS, was consistent with both ^{13}C and ^{1}H NMR spectral data (Table 3). Comparison of the spectroscopic data (UV, IR, and 1D NMR) revealed **8** was the analogue of **7**. Their ^{1}H and ^{13}C NMR spectra (Table 3) were almost identical except that the signals for OCH_3-8 were absent and a reactive hydrogen proton at δ 6.18 ppm was observed in the ^{1}H NMR spectrum. A correlation between OH-9 and H-2 was observed in the different NOE experiments (Figure 2C). Thus, the structure of **8** was established as the OH-8 analogue of **7**.

Decomposition Studies of Citrinin (13). Because citrinin (**13**) is a well-known contaminant of a number of agricultural products, many studies have been carried out on its detoxification via degradation. Known citrinin decomposition products include the monomeric derivatives phenol A (**16**),[10,14] phenol A acid,[14] decarboxycitrinin,[14] and citrinin H2,[25,26] and the dimers citrinin H1[27] and dicitrinin A (**11**).[14] It indicated that the citrinin derivatives we isolated could be artifacts as a result of handling and/or storage. To investigate the artificial nature of the derivatives, a decomposition study was performed. To a sample of

dx.doi.org/10.1021/jm200511x |J. Med. Chem. 2011, 54, 5796–5810

Table 4. In Vitro Cytotoxicity of Compounds 1−16 in Three Tumor Cell Lines [a]

compd	HL60 (IC_{50}, μM)[b]	HCT116 (IC_{50}, μM)[b]	KB (IC_{50}, μM)[b]
1	5.98 ± 2.61	4.54 ± 1.59	5.05 ± 2.31
2	6.06 ± 1.94	5.80 ± 0.76	5.15 ± 0.09
3	8.17 ± 1.86	8.57 ± 2.02	>10
4	3.20 ± 0.90	4.82 ± 1.68	3.87 ± 1.09
5	8.91 ± 1.27	>10	>10
6−16	>10	>10	>10

[a] The cell growth rate was evaluated after 72 h by SRB or MTT assay. [b] IC_{50} is the concentration that causes 50% growth inhibition. Values represent means ± SD of three individual experiments.

50 mg of citrinin (**13**) was added 0.5 mL of MeOH. The mixture was stirred at room temperature for 30 days. The reaction was monitored by HPLC-PDA-MS and TLC analyses (Supporting Information Figure F23). As shown, several monomeric species (**15** and **16**) and dimers (**1**, **2**, **6**, **9**, **10**, and **11**) were detected, which were further identified by comparison of retention time with the pure compounds.

On the basis of the decomposition results, a plausible mechanism for dimerization and trimerization of citrinin (**13**) is proposed (Supporting Information Figure F25). Citrinin (**13**) exists as a resonance hybrid between two extreme structures, *p*-quinone and *o*-quinone, either in solution or in the solid state.[30,31] A heterocyclic Diels−Alder connection between a *p*-quinone and an *o*-quinone, and the subsequent pathway to form the 8, 8′-oxygen-bridged dimers, penicitrinol B (**9**), penicitrinol A (**10**), dicitrinin A (**11**), and penicitrinone B (**12**), have been proposed by Clark, B. R, et al.[14−16,27] We also found that penicitrinol B (**9**) was unstable in MeOH and partially transformed into **7** and **8** during storage (Supporting Information Figure F24 and F25). The 6, 8′-oxygen-bridged dimers **2** and **6** and trimer **4** were proposed to derive from an unprecedented heterocyclic Diels−Alder dimerization between two *o*-quinones of **13**, according to Clark's hypothetic pathway of their 8, 8′-oxygen-bridged isomers (Supporting Information Figure F25).[14] Thus, all the isolated citrinin derivatives (**1**−**4** and **6**−**16**) were postulated to be artifacts and their absolute configurations were deduced as shown (Figures 1, 2, and Supporting Information F25).

Citrinin Derivatives Inhibit Cancer Cell Proliferation in Vitro. To evaluate the in vitro antitumor effects of citrinin derivatives (**1**−**16**), MTT and SRB assays were performed to examine their proliferative inhibition activity against three tumor cell lines: HL60, HCT116, and KB. Citrinin dimers **1**, **2**, and **5** as well as trimes **3** and **4**, all bearing a pyran ring A system in structure, displayed potent cytotoxicity with low-micromolar IC_{50} values (Table 4). In comparison, other dimers bearing a furan ring A system (**6**−**12**) as well as all the citrinin monomeric analogues (**13**−**16**) exhibited no cytotoxicity (IC_{50} > 10 μM) in the tested cell lines. The results suggest that the pyran ring A system in the Diels−Alder coupling citrinin dimers or trimers is essential for their in vitro cytotoxicity. Tricitrinol B, which exhibited the most potent cytotoxic effects (Table 4) was picked out for further studies.

Tricitrinol B (4) Shows Extensive Cytotoxicity in Tumor Cell Lines and Potential Anti-Multidrug Resistance Capabilities. *Tricitrinol B Exhibits Antiproliferative Activity in Tumor Cells.* To examine the broad-spectrum antitumor activity of tricitrinol B (**4**), MTT and SRB assays were employed against a panel of 17 human cell lines, including leukemia, colon cancer, liver cancer, gastric cancer, lung cancer, melanoma, breast cancer, ovarian cancer, prostate cancer, cervical cancer, epidermoid cancer, rhabdomyosarcoma, and normal cell line HMEC (human microvascular endothelial cell). As shown in Figure 4A, tricitrinol B (**4**) displayed potent and comparable cytotoxicity in the 16 tested tumor cell lines, with an average IC_{50} value of 4.83 μM, indicating that tricitrinol B (**4**) possessed broad-spectrum in vitro antitumor activities. In addition, the IC_{50} value of tricitrinol B against normal cell line HMEC was 7.89 ± 1.26 μM, which was almost twice as much as against tumor cells.

Tricitrinol B Overcomes Drug Resistance. Multidrug resistance (MDR) is a notorious nature of tumors and is a significant impediment to the success of cancer chemotherapy with naturally derived anticancer drugs.[32] P-glycoprotein (P-gp) overexpression is reported as a major MDR mechanism.[32] To test the antimultidrug resistance capability of tricitrinol B (**4**), two P-gp-overexpressed tumor cell lines MCF-7/ADM and KB/VCR and their normal conterparts were employed. High degrees of drug resistance was observed for the two reference compounds adriamycin (RF = 173.77, Figure 4B) and vincristine (RF = 55.97, Figure 4B). Tricitrinol B (**4**) displayed totally equipotent cytotoxicity in MDR cells and their corresponding parental cells, with RF values of 1.28 and 0.94 (Figure 4B). The results indicate that tricitrinol B (**4**) is not a substrate of the P-gp pump and has potential antimultidrug resistance capabilities.

Tricitrinol B (4) Induces HL60 and HCT116 Cell Apoptosis via Mainly Extrinsic Pathway and Induces G2/M Arrest. *Tricitrinol B Induces Cell Apoptosis.* Apoptosis is one of the important ways that chemotherapeutic drugs kill tumor cells.[32−36] DNA ladder assay was applied to explore if the antiproliferative activity of tricitrinol B (**4**) is related to apoptosis. As shown in Figure 5A, tricitrinol B (**4**) triggered DNA fragmentation of HL-60 cells in a dose-dependent manner, suggesting apoptosis is the main death type caused by tricitrinol B (**4**). To further characterize the apoptosis induced by tricitrinol B (**4**), Annexin V−PI assay was used to quantitate the apoptotic cells of HL60. As illustrated in Figure 5B, the proportion of apoptotic cells increased from ∼10% to ∼60% when exposed to 2.5−10 μM of tricitrinol B (**4**) for 24 h, and time-course test got similar results. It indicated tricitrinol B (**4**) could induce HL60 cell apoptosis in a dose-dependent and time-dependent manner.

Tricitrinol B Drives Apoptosis mainly via Extrinsic Pathway. We then evaluated whether tricitrinol B (**4**) induced apoptosis in a caspase-dependent manner. We preferentially examined the impact of tricitrinol B (**4**) on procaspase-3 (an indicator of caspase-3 activity) and PARP (a downstream target of caspase). The results showed that tricitrinol B (**4**) dose-dependently decreased the expression of procaspase-3 and increased the cleaved-caspase-3 in two cell lines (Figure 5C). In addition, tricitrinol B (**4**) resulted in PARP cleavage in a dose-dependent fashion, as evidenced by an increase in 85 kDa of inactive intermediate band of PARP with a concomitant decrease in 116 kDa of the full length (Figure 5C). After tricitrinol B (**4**) treatment for 24 h, caspase-9, which has been proposed as the initiator caspase in mitochondrial-dependent apoptotic pathway, and caspase-8, which is identified as the apical caspase in apoptosis induced by death receptors, were both activated in HL60 and HCT116 cells (Figure 5C). These findings favor involvement of both extrinsic and intrinsic apoptosis pathways in the tricitrinol B-mediated cleavage of caspase-3. Instead of directly cleaving caspase-3, activated caspase-8 could also cleave Bid into two

A

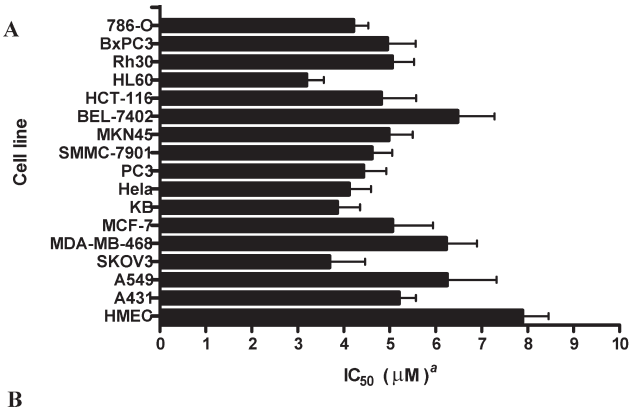

B

Compd.	IC_{50} (μM)[a]		RF[b]	IC_{50} (μM)[a]		RF[b]
	MCF-7	MCF-7/ADR		KB	KB/VCR	
Tricitrinol B (**4**)	5.76±0.66	7.41±0.84	1.28	4.91±0.89	4.60±0.54	0.94
ADR	0.25±0.10	43.44±3.49	173.77	NT[c]	NT[c]	NT[c]
VCR	NT[c]	NT[c]	NT[c]	0.02±0.01	1.29±0.10	55.97

Figure 4. In vitro cytotoxicity of tricitrinol B (**4**) in 17 cell lines (A) and inhibition of two pairs of multidrug-resistant tumor cell lines (B). The cell growth rate was evaluated after 72 h by SRB assay. [a]IC_{50} is the concentration that causes 50% growth inhibition. Values represent means ± SD of three individual experiments. [b]Relative resistance index (RF) = IC_{50} (drug-resistant)/IC_{50} (drug-sensitive). [c]Activity not tested.

fragments, then C-terminal fragment relocates from cytosol to mitochondria and promotes the activation of caspase-9, finally inducing cellular apoptosis.[37] As shown in Figure 5C, tricitrinol B (**4**)-driven apoptotic events were also associated with cleavage of Bid, indicating that extrinsic pathways may mainly involve in the apoptosis induced by tricitrinol B (**4**). Using specific inhibitors of caspase-8, -9, and pan-caspase inhibitor 2 h prior to treatment with tricitrinol B (10 μM, 24 h), we found that Z-VAD-FMK- (pan-caspase inhibitor) completely abolished the cleavage of PARP, Z-IETD-FMK (caspase-8 inhibitor) had partial effect (may be due to compensation mechanism), but Z-LEHD-FMK (caspase-9 inhibitor) failed to block those apoptotic events (Figure 5D). Taken together, the data exhibited capability of tricitrinol B (**4**) to induce apoptosis in both suspension cells HL60 and adherent cells HCT116 via mainly extrinsic pathway.

Tricitrinol B Induces G2/M Arrest. G2/M arrest is another factor for inhibition of proliferation. Perturbation of the cell cycle by a 24 h drug treatment was assessed by flow cytometry. As tricitrinol B concentration increased from 0 to 5 μM, the proportion of G2/M phase cells increased from 24.23% to 42.06% (Figure 5E).

Tricitrinol B (4) Inhibits the Catalytic Activity of Topo IIα and Induces DNA Damage. To identify the cellular molecular target(s) of tricitrinol B, we put it through our existing screening platform consisting of cellular biological molecules common to tumor cells, including topoisomerases. Tricitrinol B (**4**) revealed excellent repeatability of its inhibitory activity on human topo IIα in different tested experimental models.

Tricitrinol B Inhibits the Catalytic Activity of Topo II. In a biochemical assay for topo IIα-mediated relaxation of pBR322 DNA, tricitrinol B (**4**) reduced pBR322 relaxation in a concentration-dependent manner (Figure 6A). This topo IIα inhibition of tricitrinol B (**4**) was further confirmed by topo II-specific, enzyme-mediated kDNA decatenation assays. As shown in Figure 6B, tricitrinol B (**4**) apparently suppressed topo II-catalyzed decatenation of kinetoplast DNA in the presence of ATP in a concentration-dependent manner. These data suggest that tricitrinol B (**4**) is a topo II inhibitor.

Tricitrinol B Intercalates into DNA. DNA intercalation is an important feature of some topo II inhibitors such as adriamycin (ADM) and amsacrine (m-AMSM), which could intercalate into DNA or bind to the minor groove of DNA. But some other topo II inhibitors, i.e. etoposide, do not insert into DNA double strands.[38] Therefore, we investigated whether tricitrinol B is a DNA intercalator by detecting its ability to unwind linearized pBR322. As indicated in Figure 6C, the positive reference adriamycin gave rise to obvious inhibition of T4 ligase activity due to its strong DNA intercalative ability;[39] tricitrinol B had a similar but weaker effect, indicating that tricitrinol B is an intercalating topo II inhibitor.

Tricitrinol B Interferes with Pre- and Poststrand Passage DNA Cleavage/Religation Equilibria in the Catalytic Cycle. Following the binding to DNA, topo IIα cleaves a double helix, which allows the passage of a second DNA segment through the break and eventually reunites the strand breaks, thus removing DNA superhelices by decreasing the linking number by two each time. This process is central to the catalytic cycle of the enzyme.[40] Divalent cations and ATP are critical for this topo IIα-mediated progression. The presence of calcium and magnesium drives topo IIα to establish a DNA cleavage/religation equilibrium. This is called the prestrand-passage equilibrium to distinguish itself from the cleavage/religation equilibrium established after the strand passage event driven by the addition of ATP. Therefore, by adding 1 mM App (NH) p (an ATP analogue) or not, we experimentally set up the enzyme-mediated pre- and poststrand passage DNA cleavage/religation equilibria. Tricitrinol B apparently enhanced topo IIα-mediated DNA cleavage both before (Figure 6D) and after DNA strand passage (Figure 6E). Concurrently, tricitrinol B suppressed topo IIα-mediated DNA religation both before (Figure 6F) and after the DNA strand passage (Figure 6G). All these actions of tricitrinol B revealed an excellent concentration-dependent relationship. It is important to note that tricitrinol B clearly impaired the poststrand-passage equilibrium more than the prestrand-passage event. The results indicate that tricitrinol B can break the topo IIα-mediated DNA cleavage/religation equilibria, which might increase the amount of broken DNA.

dx.doi.org/10.1021/jm200511x |*J. Med. Chem.* 2011, 54, 5796–5810

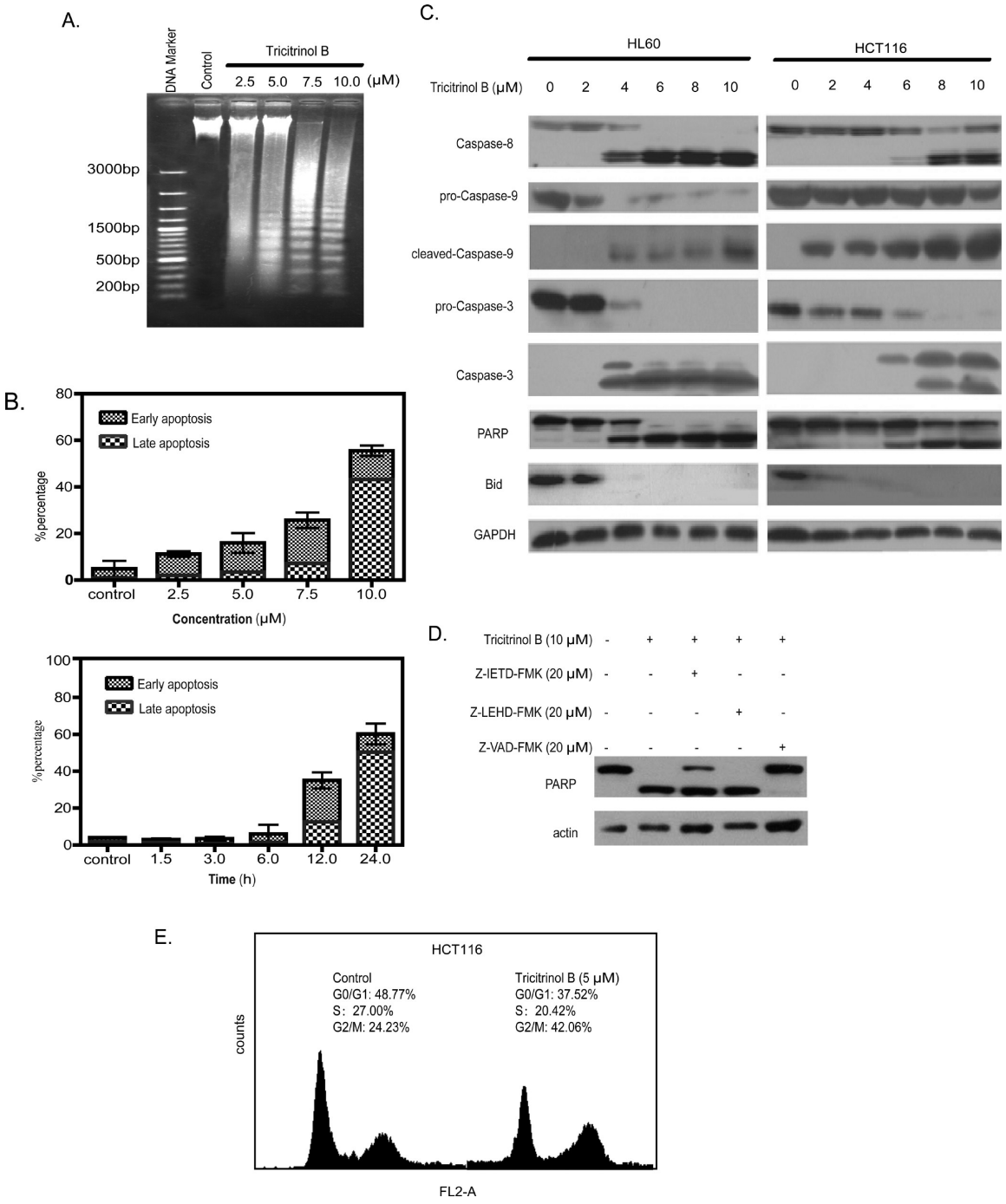

Figure 5. Tricitrinol B (**4**) induced tumor cell apoptosis. (A) Effects of tricitrinol B on the DNA ladder formation. HL60 cells were incubated with 2.5, 5.0, 7.5, or 10.0 μM tricitrinol B for 24 h. Results are a representative of three separate experiments. (B) Determination of apoptotic cell fractions by flow cytometric analysis. HL60 cells incubated with tricitrinol B (2.5−10 μM) for 24 h or with tricitrinol B (10 μM) for indicated time were fixed and stained with Annexin and PI. Percentage of early or late apoptotic cells were determined by flow cytometry Results represent means ± SD of three individual experiments. (C) Concentration-dependent caspases activation is involved in tricitrinol B-induced apoptosis in both HL60 and HCT116 cells. Whole cell lysates were prepared after being incubated with tricitrinol B (2.5−10 μM) for 24 h. Signals of processed proteins were detected by Western blotting with antibodies specific to caspase-3, -8, and -9, PARP, and Bid. Data shown are representative of three independent experiments with similar results. (D) Caspase inhibitors attenuated tricitrinol B-induced cleavage of pro-caspase-3 and PARP. HL60 cells were cultured with 10 μM tricitrinol B for 24 h with or without pretreatment with 20 μM Z-IETD-FMK, Z-LEHD-FMK, or Z-VAD-FMK for 1 h. The three independent experiments yielded similar and typical results. (E) HCT116 cells treated with or without tricitrinol B (5 μM) for 24 h were assayed by flow cytometry after staining with PI. The data were representative of three independent experiments.

Tricitrinol B Triggers DNA Double-Strand Breaks. Topo II poisons could generate irreversible DNA double-strand breaks, while topo II catalytic inhibitors could not. To test the capability of tricitrinol B (**4**) to induce DNA double-strand breaks, the phosphorylated histone H2AX (γ-H2AX), a well-known DSBs molecular marker, was checked. As shown in Figure 6H, tricitrinol B (**4**) increased the expression of γ-H2AX in both dose- and time-dependent manners. All the results together

dx.doi.org/10.1021/jm200511x |*J. Med. Chem.* 2011, 54, 5796–5810

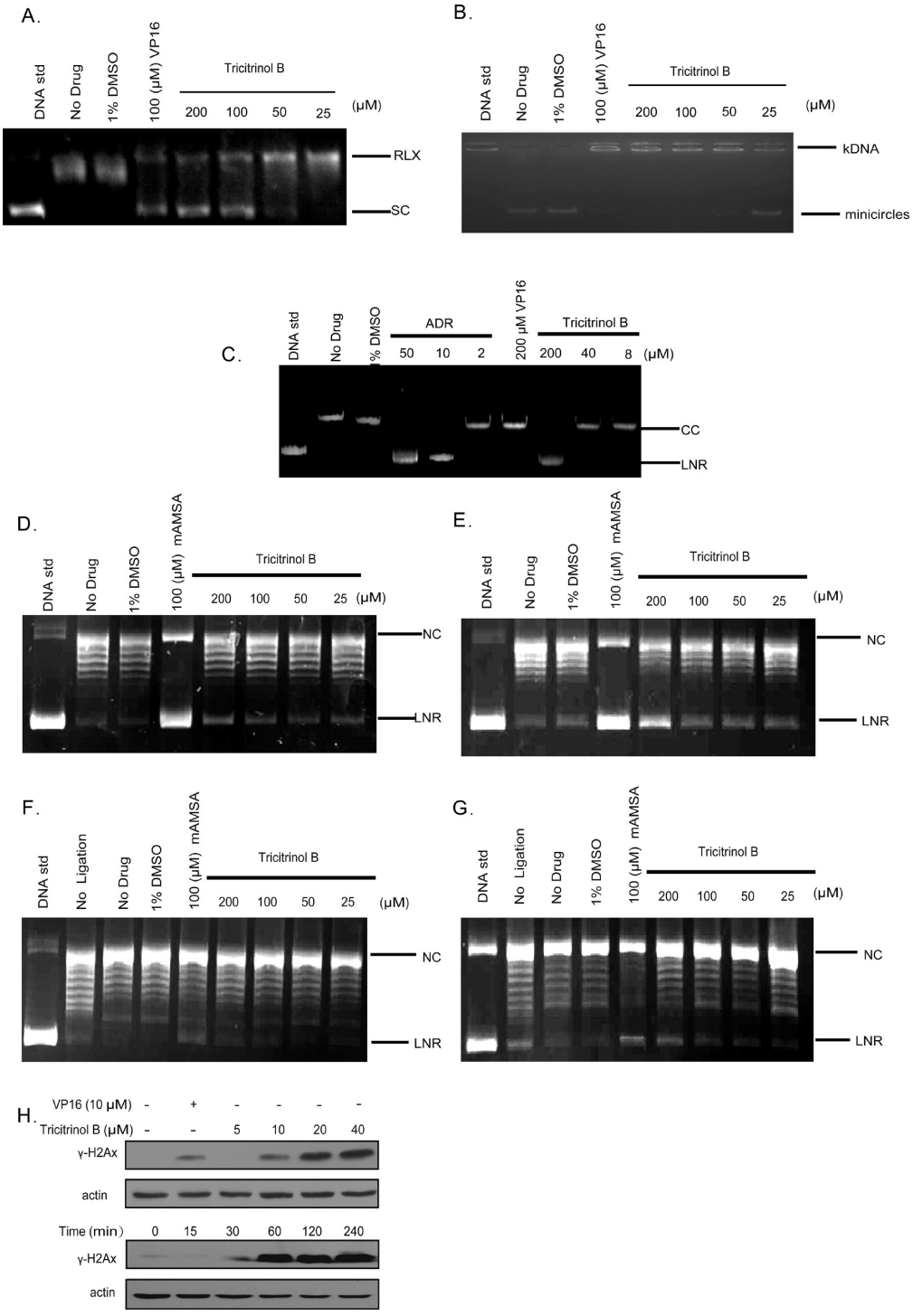

Figure 6. Tricitrinol B (**4**) is a topoisomerase IIα (topo IIα) inhibitor. (A) Tricitrinol B (**4**) inhibited topo IIα-mediated supercoiled DNA relaxation. Negatively supercoiled pBR322 (SC) and relaxed DNA (RLC) were shown by electrophoresis on an agarose gel after tricitrinol B (**4**) treament at the indicated concentration. VP16 was used at 100 μM as the positive control. (B) Topo IIα-mediated kDNA decatenation was inhibited by tricitrinol B (**4**). The position of kDNA and minicircles were indicated. (C) DNA unwinding assays with T4 ligase were performed. The images were representative of three independent experiments with similar results (ADR, adriamycin; LNR, linear form; CC, circularized form). Adriamycin gave rise to obvious inhibition on T4 ligase activity due to its strong DNA intercalative ability; tricitrinol B showed similar but weaker inhibition on T4 ligase activity. (D,E) The effects of tricitrinol B on the prestrand (D) and poststrand (E) passage topo II-mediated DNA cleavage were examined as described in the Experimental Section. Negatively supercoiled pBR322 (DNA Std) was shown for reference. The position of linear DNA (LNR) and nicked DNA (NC) were indicated. (F) and (G), The effects of tricitrinol B on prestrand (F) and poststrand (G) passage topo II-mediated DNA religation were examined as described in the Experimental Section. (H) Tricitrinol B (**4**) induced γ-H2Ax elevation in a concentration-depengdent or time-dependent manner. HL60 cells were treated with tricitrinol B (5−40 μM) for 1 h or treated with 20 μM of tricitrinol B for indicated time. The data were representative of three independent experiments.

dx.doi.org/10.1021/jm200511x |*J. Med. Chem.* 2011, 54, 5796–5810

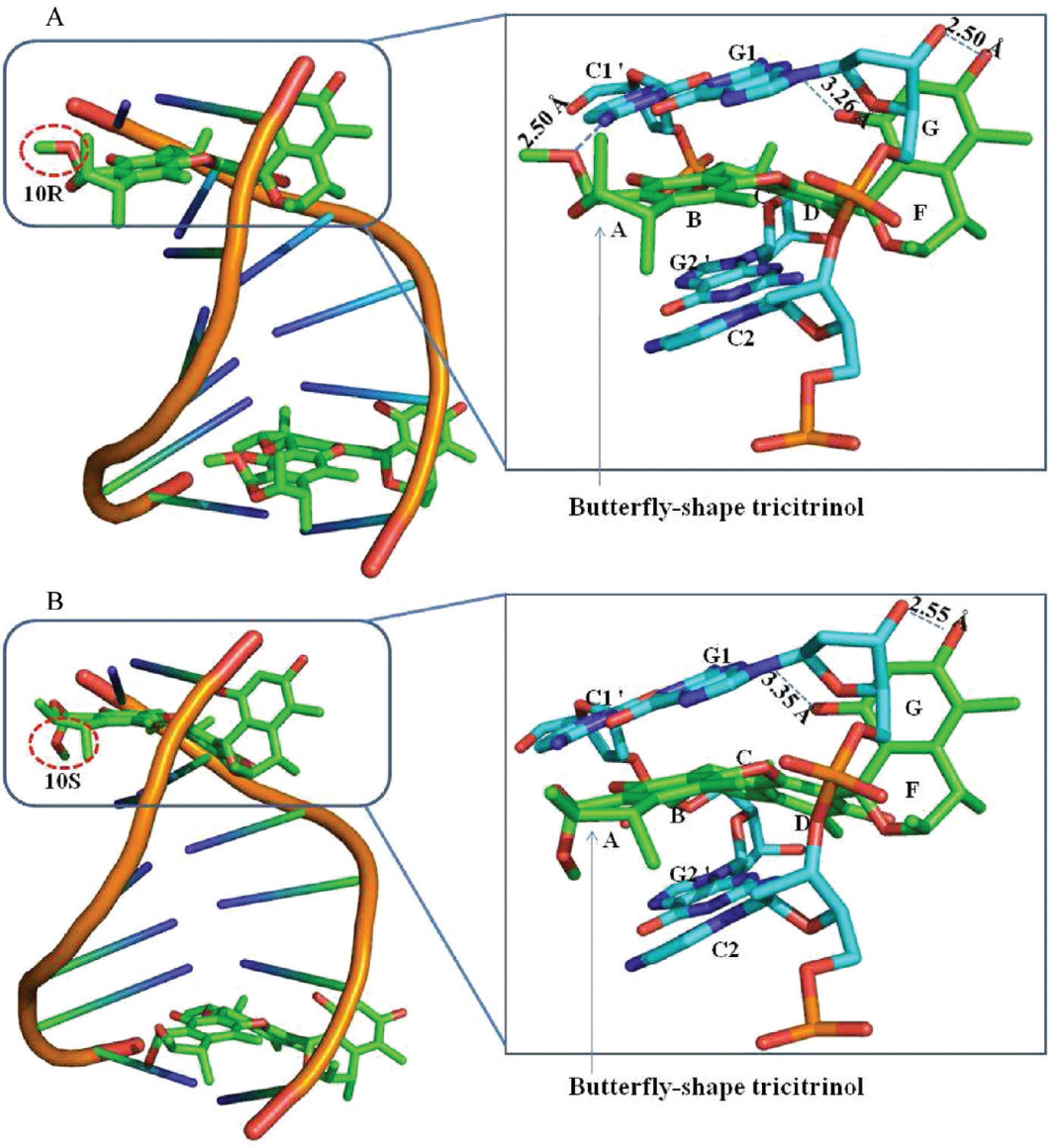

Figure 7. Docking of tricitrinol B (**4**) into DNA. (A) Binding mode of 10*R* epimer with DNA. (B) Binding mode of 10*S* epimer with DNA. The DNA structure is 1NAB, in which two tricitrinol B (**4**) molecules are bound to DNA. Tricitrinol B (**4**) and its interacting base pairs are depicted as a stick drawing. Hydrogen atoms are not shown for clarity.

demonstrate that tricitrinol B (**4**) possesses potent topo IIα inhibitory activity and can induce DNA damage, which suggest that tricitrinol B (**4**) functions as an intercalating topo IIα poison.

Molecular Modeling and Docking. The molecular modeling and docking was carried out to ascertain the possibility of tricitrinol B (**4**) (10*S* and 10*R*) to bind to the intercalation site of a six-base pair X-ray crystal structure of two molecules of an anthracycline separated by four base pairs intercalated into double-stranded DNA, using the genetic algorithm docking program GOLD version 5.0. Gold docking scores were shown to be good at predicting the binding modes of DNA with anthracyclines and their derivatives.[41,42] In DNA/anthracycline complex structure, the large outward bulges associated with the base pairs directly above and below it, induced by the planar anthracycline molecule, were observed.[41,42] The resulting docking models reveal that binding of 10*R* and 10*S* epimers of tricitrinol B (**4**) to d $(CGTACG)_2$ is characterized by classical features of anthracycline–DNA interactions. Two tricitrinol B (**4**) molecules bisintercalated into two intercalation sites with equivalent binding mode. In tricitrinol B into a beautiful butterfly shape pseudo plane (Figure 7). Therefore, tricitrinol B (**4**) could be accommodated by the structure of DNA. In each site, the butterfly shaped pentacyclic head intercalates between −1 and +1 bases, and the tail part (rings F and G) interacts with the minor groove by forming strong hydrogen bond and hydrophobic interactions. The docking produced chemically reasonable bisintercalation complexes which are shown in Figure 7. Though tricitrinol B (**4**) does not have the exact plane of an anthracycline, which is highly coplanar with the base pairs of DNA hexamers, the overall structures of tricitrinol B (**4**) complexes are similar to those of anthracyclines with DNA hexamers. The pseudoplane pentacyclic rings could be reasonably accommodated by the intercalation sites of DNA. It is noteworthy that ring B in both

epimers is coplanar and forms strong $\pi-\pi$ stacking interaction with the base pairs of DNA. Furthermore, ring G contributes to the affinity with DNA by forming both hydrogen bond and hydrophobic interactions. Interestingly, the methoxy group in the 10*R* epimer forms strong hydrogen bond interaction with cytosine, while it points to another side in the 10*S* epimer (Figure.7). Though it is hard to separate the two epimers, the docking results show that the DNA binding ability of the 10*R* epimer should be stronger than that of the 10 *S* epimer. Because of insufficient knowledge of a intercalator−DNA−topoisomerase II complex structure, the exact mechanism of actions of tricitrinol B (**4**) could not be fully understood. However, the current binding study of tricitrinol B with DNA is allowed for rational design of more new-scaffold intercalators with high affinity to DNA. Especially, the tail part (rings F and G) may have a key influence on the binding with DNA.

CONCLUSION

In summary, on the basis of the cytotoxic screening of 16 citrinin derivatives, we have found two citrinin trimers (**3** and **4**) and three citrinin dimers (**1**, **2**, and **5**), all of which possess essential six-membered ring A systems, exhibiting potent cytotoxicities. Our study has also identified tricitrinol B (**4**), with an unprecedented skeleton, as an interesting lead topo IIα inhibitor. This compound displays broad-spectrum in vitro antitumor effects and potential antimultidrug resistance capabilities. Furthermore, it could induce apoptosis in both suspension and adherent tumor cell lines via mainly extrinsic pathway. Comprehensive antitumor mechanism study and computational docking analysis indicated that tricitrinol B (**4**) functions as an intercalating topoisomerase II poison which inhibits the enzyme activity of topo IIα and induces DNA damage by stabilizing topo IIα/DNA complex. Overall, this work affords a novel structural skeleton for developing new topo II inhibitors.

EXPERIMENTAL SECTION

General. Melting points were measured by a Yanaco MP-500D micromelting point apparatus and were uncorrected. Specific rotations were obtained on a JASCO P-1020 digital polarimeter. UV spectra were recorded on Beckman DU 640 spectrophotometer. IR spectra were taken on a NICOLET NEXUS 470 spectrophotometer in KBr discs. ^{1}H, ^{13}C NMR, and DEPT spectra and 2D-NMR were recorded on a JEOL JNM-ECP 600 spectrometer using TMS as internal standard, and chemical shifts were recorded as δ values. ESI-MS were measured on a Q-TOF ULTIMA GLOBAL GAA076 LC mass spectrometer. HPLC was performed on a Waters system, equipped with a 600 controller and a 996 photodiode array detector. Semiprepartive HPLC was performed using a C-18 ODS column [YMC-pak ODS-A, 10 mm × 250 mm, 5 μm, 4 mL/min]. Different isocratic or gradient solvent systems comprised of MeOH/H_2O or MeCN/H_2O were used to generate the best resolution of each compound. The purity of all compounds was judged by the percentage of the integrated signal at UV 205 nm. All final compounds submitted for bioassay were at least 95% pure as judged by this method.

Fungal Material. *P. citrinum* HGY1−5 was isolated from crater ash collected from the extinct volcano Huguangyan in Guangdong, China. It was identified according to its ribosomal internal transcribed spacers and the 5.8S rRNA gene (ITS1−5.8S-ITS2). A voucher specimen is preserved in the China Center for Type Culture Collection (patent depository number: CCTCC M 208170). The working strain was prepared on Potato Dextrose agar slants and stored at 4 °C.

Fermentation, Extraction, and Isolation. Spores were directly inoculated into 500 mL Erlenmeyer flasks containing 100 mL of fermentation media (mannitol 20 g, maltose 20 g, glucose 10 g, monosodium glutamate 10 g, KH_2PO_4 0.5 g, $MgSO_4 \cdot 7H_2O$ 0.3 g, yeast extract 3 g and corn steep liquor 1 g, dissolved in 1 L water, pH 6.5). The flasks were incubated on a rotatory shaker at 165 rpm at 28 °C. After 15 days of cultivation, 40 L of whole broth was filtered through cheesecloth to separate broth supernatant and mycelia. The former was extracted with EtOAc and *n*-butanol in succession. The two extracts were concentrated in vacuo to give an EtOAc gum (27 g) and a *n*-butanol gum (100 g), respectively.

The EtOAc gum was subjected to Si gel column chromatography (CC, $CHCl_3$-MeOH, v/v, gradient) and the fraction FY-2 eluted with the solvent of $CHCl_3$-MeOH (20:1) was subjected to repeated chromatography on Sephadex LH-20 CC ($CHCl_3$−MeOH, 1:1). Subfraction FY-2-1-1 was recrystallized in MeOH to give compound **13** (500 mg). Subfraction FY-2-1-2 was further purified by HPLC (MeOH-H_2O, 65:35) to give compounds **11** (69 mg) and **12** (87 mg). Compound **14** (26 mg) was separated from subfraction FY-2-1-3 by HPLC eluted with MeOH−H_2O 35:65.

The *n*-butanol gum was subjected to Si gel CC (petroleum ether−acetone, $CHCl_3$−MeOH, v/v, gradient) to give 12 fractions. Fractions FZ-3 (eluted with the solvent of petroleum ether−acetone 10:1), FZ-5 (eluted with the solvent of petroleum ether−acetone 10:1), FZ-6 (eluted with the solvent of $CHCl_3$), and FZ-7 (eluted with the solvent of $CHCl_3$−MeOH 20:1) were subjected to repeated chromatography on Sephadex LH-20 CC ($CHCl_3$−MeOH, 1:1), respectively. Subfraction FZ-3-1-5 was further purified by HPLC (MeOH−H_2O, 60:40) to give compounds **7** (30 mg) and **8** (32 mg). Compounds **6** (26 mg) and **9** (35 mg) were separated form subfraction FZ-5-2-1 by HPLC eluted with MeOH−H_2O 70:30. Similar purification of subfractions FZ-5-2-2 (HPLC eluted with CH_3OH−H_2O 80:20), FZ-6-1-2 (HPLC eluted with MeOH−H_2O 45:55), FZ-6-2-2 (HPLC eluted with MeOH−H_2O 45:55), FZ-7-1-1 (HPLC eluted with MeOH−H_2O 80:20), FZ-7-1-2 (HPLC eluted with MeOH−H_2O 75:25), FZ-7-2-2 (HPLC eluted with MeOH−H_2O 85:15), and FZ-7-2-3 (HPLC eluted with MeOH−H_2O 80:20), gave compounds **10** (41 mg), **15** (35 mg), **16** (65 mg), **1** (164 mg), **2** (89 mg), **3** (78 mg), and **4** (102 mg), respectively.

Acidic Transformation of Compound 1. To a suspension of 30 mg of **1** in 0.5 mL DMSO was added 50 μL of TFA at room temperature. The color of the mixture turned into deep-red immediately. Then 5 mL of H_2O was added, and the mixture was extracted with 3 × 5 mL EtOAc. The EtOAc solution was dried on anhydrous Na_2SO_4, evaporated at reduced pressure, and the residue was subjected to Sephadex LH-20 CC ($CHCl_3$−MeOH, 1:1), and HPLC (MeOH−H_2O, 75:25) to give **5** (15 mg, 54.1% yield).

Decomposition Study of Citrinin (13). Citrinin (**13**) (50 mg) was dissolved in MeOH (0.5 mL). The mixture was stirred at room temperature for 30 days. The reaction was monitored by HPLC-PDA-MS and TLC analyses. The products were also identified by comparison of the retention time with the standards. (HPLC conditions: 0−30 min, 20% MeCN/H_2O to 90% MeCN/H_2O; 30−40 min, 90% MeCN/H_2O; 200 nm; 1 mL/min. TLC conditions: solvent, $CHCl_3$:MeOH = 10:1; Ingrain agents, H_2SO_4−vanillin).

Dicitrinol A (1). Yellowish solid (methanol); mp 208−210 °C; $[\alpha]^{25}_D$ −34.3 (*c* 0.53, MeOH). UV (MeOH) λ_{max} (log ε) 211(4.65), 221 (4.66), 294 (3.69) nm. IR ν_{max} (KBr) 3419, 3333, 2970, 2929, 2891, 1640, 1611, 1590, 1510, 1472, 1387, 1334, 1270, 1178, 1135, 1088, 1038, 1012, 950, 837 cm^{-1}. ^{1}H NMR and ^{13}C NMR data, see Table 1. HRESIMS $[M - H]^-$ *m*/*z* 425.1954 (calcd for $C_{25}H_{29}O_6$, 425.1964).

Dicitrinol B (2). Yellowish solid (methanol); mp 243−245 °C; $[\alpha]^{25}_D$ −104.4 (*c* 0.59, MeOH). UV (MeOH) λ_{max} (log ε) 221 (4.69), 295 (4.04) nm. IR ν_{max} (KBr) 3335, 2970, 2929, 2876, 2826, 1638, 1610, 1586, 1495, 1380, 1344, 1261, 1128, 1073, 1044, 959, 905, 840 cm^{-1}. ^{1}H NMR and ^{13}C NMR data, see Table 1. HRESIMS $[M - H]^-$ *m*/*z* 425.1980 (calcd for $C_{25}H_{29}O_6$, 425.1964).

Tricitrinol A (3). Yellowish solid (methanol); mp 235−237 °C; $[\alpha]^{25}_D$ −109.9 (*c* 0.29, MeOH). UV (MeOH) λ_{max} (log ε) 211 (4.89),

dx.doi.org/10.1021/jm200511x | J. Med. Chem. 2011, 54, 5796–5810

291 (4.07) nm. IR ν_{max} (KBr) 3419, 2969, 2929, 2877, 1640, 1595, 1453, 1378, 1326, 1288, 1250, 1131, 1049, 912, 834 cm^{-1}. ^1H NMR and ^{13}C NMR data, see Table 2. HRESIMS $[M - H]^-$ m/z 631.2894 (calcd for $C_{37}H_{43}O_9$, 631.2907).

Tricitrinol B (4). Yellowish solid (methanol); mp 237−239 °C; $[\alpha]^{25}_D$ −141.5 (c 0.15, MeOH). UV (MeOH) λ_{max} (log ε) 207 (4.84), 293 (4.06) nm. IR ν_{max} (KBr) 3438, 3297, 2972, 2930, 2872, 2820, 1637, 1592, 1456, 1374, 1323, 1264, 1119, 1048, 968, 948, 898 cm^{-1}. ^1H NMR and ^{13}C NMR data, see Table 2. HRESIMS $[M - H]^-$ m/z 631.2879 (calcd for $C_{37}H_{43}O_9$, 631.2907).

Oxodicitrinol A (5). Yellow solid (methanol); $[\alpha]^{20}_D$ +30.5 (c 0.15, MeOH). UV (MeOH) λ_{max} (log ε) 234 (4.23), 262 (4.22), 316 (3.75), 400 (4.02), 418 (4.02) nm. IR ν_{max} (KBr) 3445, 2969, 2930, 2867, 1641, 1603, 1570, 1516, 1456, 1376, 1287, 1197, 1154, 1099, 1069, 1006 cm^{-1}. ^1H NMR and ^{13}C NMR data, see Table 1. HRESIMS $[M - H]^-$ m/z 393.1694 (calcd for $C_{24}H_{25}O_5$, 393.1702).

Penicitrinol F (6). Yellowish solid (methanol); mp 193−194 °C; $[a]^{25}_D$ +70.6 (c 0.14, MeOH). UV (MeOH) λ_{max} (log ε) 202 (4.58), 268 (3.90), 287 (3.76), 324 (3.61) nm. IR ν_{max} (KBr) 3395, 2967, 2930, 1679, 1650, 1629, 1575, 1492, 1454, 1397, 1260, 1212, 1093, 1014, 804 cm^{-1}. ^1H NMR and ^{13}C NMR data, see Table 3. HRESIMS $[M + H]^+$ m/z 413.1955 (calcd for $C_{24}H_{29}O_6$, 413.1964).

Penicitrinol G (7). Yellow solid (methanol); mp 181−183 °C; $[a]^{25}_D$ +59.9 (c 0.66, MeOH). UV (MeOH) λ_{max} (log ε) 205 (4.54), 266 (4.03), 327 (3.70), 392 (3.83) nm. IR ν_{max} (KBr) 3444, 3404, 2967, 2930, 2872, 1650, 1596, 1563, 1455, 1377, 1314, 1258, 1187, 1104, 1016, 904, 844 cm^{-1}. ^1H NMR and ^{13}C NMR data, see Table 3. HRESIMS $[M - H]^-$ m/z 429.1905 (calcd for $C_{24}H_{29}O_7$, 429.1913).

Penicitrinol H (8). Yellow solid (methanol); mp 156−158 °C; $[a]^{25}_D$ +66.6 (c 0.52, MeOH). UV (MeOH) λ_{max} (log ε) 205 (4.53), 266 (4.01), 327 (3.69), 394 (3.85) nm. IR ν_{max} (KBr) 3439, 3417, 2969, 2932, 2899, 1649, 1597, 1561, 1455, 1398, 1370, 1315, 1259, 1198, 1109, 1081, 1053, 1012, 908, 800 cm^{-1}. ^1H NMR and ^{13}C NMR data, see Table 3. HRESIMS $[M - H]^-$ m/z 415.1705 (calcd for $C_{23}H_{27}O_7$, 415.1757).

Cell Lines and Chemicals. Human gastric cancer SGC-7901, hepatocellular carcinoma BEL-7402, and cervix adenocarcinoma HeLa cell lines were maintained in the Shanghai Institute of Materia Medica, Chinese Academy of Science (Shanghai, China). Human lung cancer cell line A549 was from the National Cancer Institute (NCI). Human leukemia HL60, oral epidermoid KB, pancreatic BxPC3, renal 786-O, breast MDA-MB-468, and epithelial carcinoma A431 cancer cell lines and human microvascular endothelial cell line HMEC were purchased from American Type Culture Collection (ATCC, Manassas, VA). Human gastric MKN45, colorectal HCT116, prostate PC3, breast MCF-7, and ovarian SKOV3 cancer cell lines were from Japanese foundation of Cancer Research (JFCR, Tokyo, Japan). The rhabdomyosarcoma cell line Rh30 was a kind gift from Dr. Houghton (St. Jude Children's Research Hospital, Memphis, TN). Adriamycin-selected multidrug resistant (MDR) cell sublines MCF-7/ADM were purchased from the Institute of Hematology, Chinese Academy of Medical Sciences (Tianjin, China). The vincristine-selected MDR KB/VCR subline was obtained from the Zhongshan University of Medical Sciences (Guangzhou, China). All these cell lines were maintained strictly according to the supplier's instructions and established procedures. Reference control durgs, like adriamycin (ADR), etoposide (VP16), vincristine (VCR), and mAMSA (amsacrine) were purchased from Sigma (St. Louis, MO).

Cytotoxicity Assays. The cytotoxicity of citrinin derivatives was examined using a panel of human cell lines. Cells were seeded into 96-well plates and treated in triplicate with gradient concentrations of citrinin derivatives at 37 °C for 72 h. Cytotoxicity in leukemia cells was tested by MTT assay as described.[43,44] SRB method was applied to check the cytotoxicity in adherent tumor cells.[45,46] The cytotoxicity of citrinin derivatives was expressed as IC_{50}, determined by the Logit method from at least three independent experiments.

Topo II-Mediated Supercoiled pBR322 Relaxation. DNA relaxation assays were employed according to the procedure as in previous studies.[47] pBR322 DNA (0.25 μg) was incubated with 0.75 unit of topo IIα (TopoGEN, Columbus, OH) at 37 °C for 30 min in 20 μL of relaxation buffer [50 mM Tris (pH 7.8), 50 mM KCl, 50 mM NaCl, 5 mM $MgCl_2$, 0.1 mM EDTA, and 15 μg/mL of bovine serum albumin (BSA), 1 mM ATP]. The reaction was terminated by adding 2 μL of 10% SDS. Electrophoresis was carried out in a 1% agarose gel in TAE at 4 V/cm for 2 h. Gel was stained with ethidium bromide and photographed under UV light.

kDNA Decatenation Assay. Topo II activity was measured by the ATP-dependent decatenation of kDNA.[48] Briefly, 0.25 μg of kDNA was incubated 0.75 unit of topo IIα at 37 °C for 30 min in 20 μL of total reaction buffer [50 mM Tris (pH 8.0), 120 M KCl, 10 mM $MgCl_2$, 0.5 mM ATP, 0.5 mM DTT, 30 μg/mL BSA]. The reaction was terminated by adding 2 μL of 10% SDS. The DNA samples were subjected to electrophoresis under the same conditions as described above.

Unwinding Assay. Unwinding assays were employed to determine whether Echinoside A could intercalate into plasmid DNA.[49] DNA unwinding effects of tricitrinol B (**4**) were assayed according to the procedure as in previous studies. Plasmid pBR322 was linearized by EcoR I restriction endonuclease and recovered by phenol and ethanol precipitation. Linearized DNA (0.1 μg) and testing compounds were incubated with 2 units of T4 DNA ligase at 22 °C for 30 min in T4 ligase buffer. The reaction was stopped by shifting the temperature to 60 °C for 10 min. The compounds were removed from the reaction mixture by extraction with phenol. The DNA samples were subjected to electrophoresis under the same conditions as described above.

Pre- and Poststrand Passage Topo II-Mediated DNA Cleavage. DNA cleavage assays were performed as described by Meng et al.[50] with minor modifications. All DNA cleavage reactions employed 6 units of topo II and 0.25 μg of supercoiled pBR322 in total volume of 20 μL of cleavage buffer that contained 5 mM $MgCl_2$. For poststrand passage DNA cleavage reactions, 1 mM APPNHP, a nonhydrolyzable form of ATP, was added to the reaction mixtures. Samples were incubated at 37 °C for 6 min and stopped by the addition of 2 μL of 10% SDS and 1 μL of a 1 mg/mL solution of proteinase K. The samples were incubated at 50 °C for 30 min to digest the enzyme. Final products were mixed with 2.5 μL of loading buffer, heated to 70 °C for 1 min, and subjected to electrophoresis in 1% agarose under the same conditions as described above.

Pre- and Poststrand Passage Topo II-Mediated DNA Religation. Topo II-mediated DNA religations were undertaken according to previous reports.[50] Reactions contained 6 units of topo II and 0.25 μg of supercoiled pBR322 in a total of 20 μL of cleavage buffer consisting 5 mM $CaCl_2$ or 1 mM APPNHP and 5 mM $MgCl_2$ for pre- and poststrand passage religation, respectively. Initial DNA cleavage/religation equilibria were established at 37 °C for 6 min. The testing samples were added to the reaction mixtures just before the initiation of DNA religation. For prestrand passage religation, the topo II−DNA cleavage complex was trapped by the addition of EDTA (0.8 μL of a 250 mM solution) and NaCl (0.6 μL of a 5 M solution) was added to prevent recleavage of the DNA. The samples were placed on ice to slow the reaction rate. Religation was initiated by the addition of 1.8 μL of cold $MgCl_2$ (8.5 mM final) and stopped by addition of 2 μL of 10% SDS. For poststrand passage religation, samples were rapidly shifted from for 5 min from 37 to 55 °C to initiate the religation, and then the reactions were terminated by the addition of 2 μL of 10% SDS. The samples were processed as described above.

PI Staining for Flow Cytometry. HCT116 cells (2×10^5 cells/mL) were treated with various concentration of tricitrinol B (**4**) for 24 h. Cells were harvested and washed with cold PBS. Then cells were fixed by

70% ethanol on ice overnight, then washed twice in PBS. For 30 min, staining occurred in PBS which contained 50 μg/mL RNase and 10 μg/mL PI at room temperature in dark. For each sample, at least 1×10^4 cells were analyzed using flow cytometry (FACSalibur, Becton Dickinson, USA).

Western Blotting. Tumor cells (2×10^5/mL) were treated with tricitrinol B (**4**) at the indicated times. The standard Western blotting was performed, and the proteins were recognized with appropriate antibodies such as pro-caspase 3, cleaved caspase 3, PARP, Bid (Santa Cruz, CA), γ-H2AX, pro-caspase-9, cleaved caspase 9, caspase 8, and Bid (Cell Signaling Technology, Beverly, MA) and visualized by ECL system.

Molecular Modeling and Docking. Molecular modeling was performed on an R14000 SGI Fuel workstation with software package SYBYL 6.9 (Tripos Inc., St. Louis, MO). Standard parameters were used unless otherwise indicated. The X-ray crystallographic structures of a 6-base pair DNA, complexed with 2 molecules of an anthracycline, d(CGTACG)/ anthracycline (http://www.rcsb.org/pdb/ PDB code: 1NAB), was retrieved from PDB. Heteroatoms and water molecules in the PDB files were removed, and all hydrogen atoms were subsequently added to the DNA with the SYBYL Biopolymer module. Three-dimensional coordinates of the 10*S* and 10*R* epimers of tricitrinol B (**4**) were generated by CORINA 3.0 (Molecular Networks GmbH, Erlangen, Germany, 2004).[51] The Gasteiger−Huckel partial charges[52] were assigned to each atom of the resultant ligand. The final conformations of the ligands were obtained after 1000 steps of energy minimization using the Tripos force field and optimization at the DFT/B3LYP/6-311G level by means of Gaussian 2009.[53]

Molecular docking was carried out using GOLD 5.0 (CCDC, Cambridge, U.K., 2010)[54] to generate an ensemble of docked conformations for the ligand. The 10*S* and 10*R* epimers of tricitrinol B (**4**) were docked into the anthracycline intercalation site of double-stranded DNA. An anthracycline (adriamycin) was docked back into its X-ray DNA structure with a heavy atom root-mean-square distance (rmsd) of 1.6 Å, showing a good predicted ability of GOLD because values of less than 2.0 Å in the GOLD test set are considered to be good.[54] Instead of the default 10600 genetic algorithm (GA) runs were performed to fully take into account the flexibility of the ligand. For each GA run, the default GA settings were used with no early termination allowed and internal ligand energy offset turned on. Finally, GOLD-Score was used as the fitness function.

■ ASSOCIATED CONTENT

Supporting Information. ^{1}H and ^{13}C NMR spectra of compounds **1**−**8**, HPLC chromatograms of **1**−**5**, and HPLC-PDA-MS and TLC analyses of the *n*-BuOH extract of *P. citrinum* HGY1−5 and the decomposition products of citrinin (**13**). This material is available free of charge via the Internet at http://pubs.acs.org.

■ AUTHOR INFORMATION

Corresponding Author

*For Q.-Q.G.: phone, +86-532-82032065; fax, +86-532-82033054; E-mail, guqianq@ouc.edu.cn. For M.-Y.G.: phone, +86-21-50806072; fax, +86-21-50806072; E-mail, mygeng@mail.shcnc.ac.cn.

Author Contributions

‖Those authors contributed equally.

■ ACKNOWLEDGMENT

This research is financially supported by the Chinese National Science Fund (no. 30973627), the State Key Laboratory of Drug Research, Shanghai Institute of Materia Medica, Chinese Academy of Sciences, the Natural Science Foundation of China for Distinguished Young Scholars (no. 30725046), National Science & Technology Major Project "Key New Drug Creation and Manufacturing Program" (nos. 2009ZX09301-001 and 2009ZX09103-045), Program of Shanghai Subject Chief Scientist (no. 10XD1405100), the Science and Technology Planning Project of Shandong Province, China (2010GSF10216), the program for Changjiang Scholars and Innovative Research Team in University (no. IRT0944)

■ ABBREVIATIONS USED

Topo, topoisomerase; DSBs, double-strand breaks; MDR, multidrug resistance; kDNA, kinetoplast DNA; DMSO, dimethylsulfoxide; SRB, sulforhodamine B; PBS, phosphate buffer saline; IC_{50}, 50% inhibitory concentration; SDS, sodium dodecyl sulfate; ADM, adriamycin; mAMSA, amsacrine; DTT, dithiothreitol; SD, standard deviation; RF, resistance factor

■ REFERENCES

(1) Denny, W. A. Chemotherapeutic effects of acridine derivatives. *Med. Chem. Rev. Online* **2004**, *1*, 257–266.

(2) Denny, W. A.; Baguley, B. C. Dual topoisomerase I/II inhibitors in cancer therapy. *Curr. Top. Med. Chem.* **2003**, *3*, 339–353.

(3) Walker, J. V.; Nitiss, J. L. DNA topoisomerase II as a target for cancer chemotherapy. *Cancer Invest.* **2002**, *20*, 570–589.

(4) Burden, D. A.; Osheroff, N. Mechanism of action of eukaryotic topoisomerase II and drugs targeted to the enzyme. *Biochim. Biophys. Acta* **1998**, *1400*, 139–154.

(5) Holden, J. A. DNA topoisomerases as anticancer drug targets: from the laboratory to the clinic. *Curr. Med. Chem.: Anti-Cancer Agents* **2001**, *1*, 1–25.

(6) Nitiss, J. L. Targeting DNA topoisomerase II in cancer chemotherapy. *Nature Rev.* **2009**, *9*, 338–350.

(7) Azarova, A. M.; Lyu, Y. L.; Lin, C. P.; Lin, C. P.; Tsai, Y. C.; Lau, J. Y. N.; Wang, J. C.; Liu, L. F. Roles of DNA topoisomerase II isozymes in chemotherapy and secondary malignancies. *Proc. Natl. Acad. Sci. U.S.A.* **2007**, *104*, 11014–11019.

(8) Newman, D. J.; Cragg, G. M. Microbial antitumor drugs: natural products of microbial origin as anticancer agents. *Curr. Opin. Invest. Drugs* **2009**, *10*, 1280–1296.

(9) Du, L.; Li, D. H.; Zhu, T. J.; Cai, S. X.; Wang, F. Z.; Xiao, X.; Gu, Q. Q. New alkaloids and diterpenes from a deep ocean sediment derived fungus *Penicillium* sp. *Tetrahedron* **2009**, *65*, 1033–1039.

(10) Du, L.; Zhu, T. J.; Liu, H. B.; Fang, Y. C.; Zhu, W. M.; Gu, Q. Q. Cytotoxic Polyketides from a Marine-Derived Fungus *Aspergillus glaucus*. *J. Nat. Prod.* **2008**, *71*, 1837–1842.

(11) Liu, R.; Lin, Z. J.; Zhu, T. J.; Fang, Y. C.; Gu, Q. Q.; Zhu, W. M. Novel open-chain cytochalsins from the marine-derived fungus *Spicaria elegans*. *J. Nat. Prod.* **2008**, *71*, 1127–1132.

(12) Du, L.; Zhu, T. J.; Fang, Y. C.; Liu, H. B.; Gu, Q. Q.; Zhu, W. M. Aspergiolide A, a novel anthraquinone derivative with naphtho[1,2,3-*de*]chromene-2,7-dione skeleton isolated from a marine-derived fungus *Aspergillus glaucus*. *Tetrahedron* **2007**, *63*, 1085–1088.

(13) Han, X. X.; Cui, C. B.; Gu, Q. Q.; Zhu, W. M.; Liu, H. B.; Gu, J. Y.; Osada, H. ZHD-0501, a novel naturally occurring staurosporine analog from *Actinomadura* sp. 007. *Tetrahedron Lett.* **2005**, *46*, 6137–6140.

(14) Clark, B. R.; Capon, R. J.; Lacey, E.; Tennant, S.; Gill, J. H. Citrinin revisited: from monomers to dimers and beyond. *Org. Biomol. Chem.* **2006**, *4*, 1520–1528.

(15) Wakana, D.; Hosoe, T.; Itabashi, T.; Okada, K.; Takaki, G. M. C.; Yaguchi, T.; Fukushima, K.; Kawai, K. New citrinin derivatives isolated from *Penicillium citrinum*. *J. Nat. Med.* **2006**, *60*, 279–284.

(16) Lu, Z. Y.; Lin, Z. J.; Wang, W. L.; Du, L.; Zhu, T. J.; Fang, Y. C.; Gu, Q. Q.; Zhu, W. M. Citrinin dimers from the halotolerant fungus *Penicillium citrinum* B-57. *J. Nat. Prod.* **2008**, *71*, 543–546.

(17) Hill, R. K.; Gardella, L. A. The absolute configuration of citrinin. *J. Org. Chem.* **1964**, *29*, 766–767.

(18) Curtis, R. F.; Hassall, C. H.; Nazar, M. The biosynthesis of phenols. Part XV. Some metabolites of *Penicillium citrinum* related to citrinin. *J. Chem. Soc. C: Org.* **1968**, *1*, 85–93.

(19) Blanc, P. J.; Laussac, J. P.; Le Bars, J.; Le Bars, P.; Loret, M. O.; Pareilleux, A.; Prome, D.; Prome, J. C.; Santerre, A. L.; Goma, G. Characterization of monascidin A from *Monascus* as citrinin. *Int. J. Food Microbiol.* **2001**, *27*, 201–213.

(20) Krogh, P.; Hasselager, E.; Friis, P. Studies on fungal nephrotoxicity. 2. Isolation of two nephrotoxic compounds from *Penicillium viridicatum* Westling: citrinin and oxalic acid. *Acta Pathol. Microbiol. Scand., Sect. B: Microbiol. Immunol.* **1970**, *78*, 401–413.

(21) Betina, V. *Mycotoxins: Chemical, Biological, and Environmental Aspects*; Elsevier: Amsterdam1989.

(22) Ammar, H.; Michaelis, G.; Lisowsky, T. A screen of yeast respiratory mutants for sensitivity against the mycotoxin citrinin identifies the vacuolar ATPase as an essential factor for the toxicity mechanism. *Curr. Genet.* **2000**, *37*, 277–284.

(23) Chagas, G. M.; Oliveira, M. B.; Campello, A. P.; Kluppel, M. L. Mechanism of citrinin-induced dysfunction of mitochondria. III. Effects on renal cortical and liver mitochondrial swelling. *J. Appl. Toxicol.* **1995**, *15*, 91–95.

(24) Yu, F. Y.; Liao, Y. C.; Chang, C. H.; Liu, B. H. Citrinin induces apoptosis in HL60 cells via activation of the mitochondrial pathway. *Toxicol. Lett.* **2006**, *161*, 143–151.

(25) Kitabatake, N.; Trivedi, A. B.; Doi, E. Thermal decomposition and detoxification of citrinin under various moisture conditions. *J. Agric. Food Chem.* **1991**, *39*, 2240–2244.

(26) Hirota, M.; Menta, A. B.; Yoneyama, K.; Kitabatake, N. A major decomposition product, citrinin H2, from citrinin on heating with moisture. *Biosci., Biotechnol., Biochem.* **2002**, *66*, 206–210.

(27) Trivedi, A. B.; Hirota, M.; Etsushiro, D.; Kitabatake, N. Formation of a new toxic compound, citrinin HI, from citrinin on mild heating in water. *J. Chem. Soc., Perkin Trans. 1* **1993**, 2167–2171.

(28) Kadam, S.; Poddig, J.; Humphpey, P.; Karwowski, J.; Jackson, M.; Tennent, S.; Fung, L.; Hochlowski, J.; Rasmussen, R.; Mcalpine, J. Citrinin hydrate and radicinin: human rhinovirus 3C-protease inhibitors discovered in a target-directed microbial screen. *J. Antibiot.* **1994**, *47*, 836–839.

(29) Barber, J.; Cornford, J. L.; Howard, T. D.; Sharples, D. The structure of citrinin in vivo. *J. Chem. Soc. Perkin. Trans. 1* **1987**, 2743–2744.

(30) Poupko, R.; Luz, Z. Carbon-13 NMR of citrinin in the solid state and in solutions. *J. Phys. Chem. A* **1997**, *101*, 5097–5102.

(31) Destro, R.; Marsh, R. E. Temperature Dependence of Tautomeric Equilibria in the Solid State: The Case of Citrinin. *J. Am. Chem. Soc.* **1984**, *106*, 7269–7271.

(32) Higgins, C. F. Multiple molecular mechanisms for multidrug resistance transporters. *Nature* **2007**, *446*, 749–757.

(33) Salvesen, G. S.; Dixit, V. M. Caspases: intracellular signaling by proteolysis. *Cell* **1997**, *91*, 443–446.

(34) Beretta, G. L.; Zunino, F. Molecular mechanisms of anthracycline activity. *Top. Curr. Chem.* **2008**, *283*, 1–19.

(35) Vial, J. P.; Belloc, F.; Dumain, P.; Besnard, S.; Lacombe, F.; Boisseau, M. R.; Reiffers, J.; Bernard, P. Study of the apoptosis induced in vitro by antitumoral drugs on leukaemic cells. *Leuk. Res.* **1997**, *21*, 163–172.

(36) Walker, P. R.; Smith, C.; Youdale, T.; Leblanc, J.; Whitfield, J. F.; Sikorska, M. Topoisomerase II-reactive chemotherapeutic drugs induce apoptosis in thymoxytes. *Cancer Res.* **1991**, *51*, 1078–1085.

(37) Li, H.; Zhu, H.; Xu, C. J.; Yuan, J. Cleavage of BID by Caspase-8 mediates the mitochondrial damage in the Fas pathway of apoptosis. *Cell* **1998**, *94*, 491–501.

(38) Brana, M. F.; Cacho, M.; Gradillas, A.; de Pascual-Teresa, B.; Ramos, A. Intercalators as anticancer drugs. *Curr. Pharm. Des.* **2001**, *7*, 1745–1780.

(39) Montecucco, A.; Pedrali-Noy, G.; Spadari, S.; Zanolin, E.; Ciarrocchi, G. DNA unwinding and inhibition of T4 DNA ligase by anthracyclines. *Nucleic Acids Res.* **1988**, *16*, 3907–3918.

(40) Fortune, J. M.; Osheroff, N. Topoisomerase II as a target for anticancer drugs: when enzymes stop being nice. *Prog. Nucleic Acid Res. Mol. Biol.* **2000**, *64*, 221–253.

(41) Hasinoff, B. B.; Liang, H.; Wu, X.; Guziec, L. J.; Guziec, F. S.; Marshall, J.; Yalowich, J. C. The structure-based design, synthesis and biological evaluation of DNA-binding bisintercalating bisanthrapyrazole anticancer compounds. *Bioorg. Med. Chem.* **2008**, *16*, 3959–3968.

(42) Zhang, R.; Wu, X.; Guziec, L. J.; Guziec, F. S.; Chee, G. L.; Yalowich, J. C.; Hasinoff, B. B. Design, synthesis and biological evaluation of a novel series of anthrapyrazoles linked with netropsin-like oligopyrrole carboxamides as anticancer agents. *Bioorg. Med. Chem.* **2010**, *18*, 3974–3984.

(43) Mosmann, T. Rapid colorimetric assay for cellular growth and survival: application to proliferation and cytotoxicity assays. *J. Immunol. Methods* **1983**, *65*, 55–63.

(44) Tao, Z.; Zhou, Y.; Lu, J.; Duan, W.; Qin, Y.; He, X.; Lin, L.; Ding, J. Caspase-8 preferentially senses the apoptosis-inducing action of NG-18, a gambogic acid derivative, in human leukemia HL60 cells. *Cancer Biol. Ther.* **2007**, *6*, 681–686.

(45) Lu, H. R.; Zhu, H.; Huang, M.; Chen, Y.; Cai, Y. J.; Miao, Z. H.; Zhang, J. S.; Ding, J. Reactive oxygen species elicit apoptosis by concurrently disrupting topoisomerase II and DNA-dependent protein kinase. *Mol. Pharmacol.* **2005**, *68*, 983–994.

(46) Skehan, P.; Storeng, R.; Scudiero, D.; Monks, A.; McMahon, J.; Vistica, D.; Warren, J. T.; Bokesch, H.; Kenney, S.; Boyd, M. R. New colorimetric cytotoxicity assay for anticancer-drug screening. *J. Natl. Cancer Inst.* **1990**, *82*, 1107–1112.

(47) Osheroff, N.; Shelton, E. R.; Brutlag, D. L. DNA topoisomerase II from *Drosophila melanogaster*. Relaxation of supercoiled DNA. *J. Biol. Chem.* **1983**, *258*, 9536–9543.

(48) Tanabe, K.; Ikegami, Y.; Ishida, R.; Andoh, T. Inhibition of topoisomerase II by antitumor agents bis(2,6-dioxopiperazine) derivatives. *Cancer Res.* **1991**, *51*, 4903–4908.

(49) Yamashita, Y.; Fujii, N.; Murakata, C.; Ashizawa, T.; Okabe, M.; Nakano, H. Induction of mammalian DNA topoisomerase I-mediated DNA cleavage by antitumor indolocarbazole derivatives. *Biochemistry* **1992**, *31*, 12069–12075.

(50) Meng, L. H.; Zhang, J. S.; Ding, J. Salvicine, a novel DNA topoisomerase II inhibitor, exerting its effects by trapping enzyme−DNA cleavage complexes. *Biochem. Pharmacol.* **2001**, *62*, 733–741.

(51) Gasteiger, J.; Rudolph, C.; Sadowski, J. Automatic generation of 3D atomic coordinates for organic molecules. *Tetrahedron Comput. Methodol.* **1990**, *3*, 537–547.

(52) Gasteiger, J.; Marsili, M. Iterative partial equalization of orbital electronegativitysa rapid access to atomic charges. *Tetrahedron* **1980**, *36*, 3219–3228.

(53) Frisch, M. J.; Trucks, G. W.; Schlegel, H. B.; Scuseria, G. E.; Robb, M. A.; Cheeseman, J. R.; Scalmani, G.; Barone, V.; Mennucci, B.; Petersson, G. A.; Nakatsuji, H.; Caricato, M.; Li, X.; Hratchian, H. P.; Izmaylov, A. F.; Bloino, J.; Zheng, G.; Sonnenberg, J. L.; Hada, M.; Ehara, M.; Toyota, K.; Fukuda, R.; Hasegawa, J.; Ishida, M.; Nakajima, T.; Honda, Y.; Kitao, O.; Nakai, H.; Vreven, T.; Montgomery, J. A., Jr.; Peralta, J. E.; Ogliaro, F.; Bearpark, M.; Heyd, J. J.; Brothers, E.; Kudin, K. N.; Staroverov, V. N.; Kobayashi, R.; Normand, J.; Raghavachari, K.; Rendell, A.; Burant, J. C.; Iyengar, S. S.; Tomasi, J.; Cossi, M.; Rega, N.; Millam, N. J.; Klene, M.; Knox, J. E.; Cross, J. B.; Bakken, V.; Adamo, C.; Jaramillo, J.; Gomperts, R.; Stratmann, R. E.; Yazyev, O.; Austin, A. J.; Cammi, R.; Pomelli, C.; Ochterski, J. W.; Martin, R. L.; Morokuma, K.; Zakrzewski, V. G.; Voth, G. A.; Salvador, P.; Dannenberg, J. J.; Dapprich, S.; Daniels, A. D.; Farkas, Ö; Foresman, J. B.; Ortiz, J. V.; Cioslowski, J.; Fox , D. J. *Gaussian 09, revision A.1*; Gaussian, Inc.: Wallingford CT, 2009.

(54) Verdonk, M. L.; Cole, J. C.; Hartshorn, M. J.; Murray, C. W.; Taylor, R. D. Improved protein−ligand docking using GOLD. *Proteins* **2003**, *52*, 609–623.